CARNAGHI, MATTHEW. Ph.D. From Memory to Processing: A Reaction-Diffusion Approach to Neuromorphic Computing. (2021)
Directed by Dr. Joseph Starobin. 63 pp.

The goal of this research is to bridge the gap between the physiological brain and mathematically based neuromorphic computing models. As such, the reaction-diffusion method was chosen as it can naturally exhibit properties like propagation of excitation that are seen in the brain, but not current neuromorphic computing models. A reaction-diffusion memory unit was created to demonstrate the key memory functions of sensitization, habituation, and dishabituation, while a reaction-diffusion brain module was established to perform the specific processing task of single-digit binary addition. The results from both approaches were consistent with existing literature detailing physiological memory and processing in the human brain.

FROM MEMORY TO PROCESSING:

A REACTION-DIFFUSION APPROACH TO NEUROMORPHIC COMPUTING

by

Matthew Carnaghi

A Dissertation

Submitted to

the Faculty of The Graduate School at

The University of North Carolina at Greensboro

in Partial Fulfillment

of the Requirements for the Degree

Doctor of Philosophy

Greensboro

2021

Approved by

Dr. Joseph Starobin
Committee Chair

DEDICATION

I would like to dedicate this dissertation to all the teachers who have helped me over the years. Without your support, I would never have made it this far. I would like to thank in particular those who have made a significant impact on my life. From Bishop McGuinness, I thank Mr. Kist and Mr. Prudhomme, who taught me to take joy from overcoming seemingly impossible challenges and sparked my love of science. From High Point University, I thank the physics and computer science departments, particularly Dr. Fiser and Dr. Titus. You taught me to stay organized and think outside the box, and to break overwhelming problems into solvable pieces. From the Joint School of Nanoscience and Nanoengineering, I thank my advisor, Dr. Starobin. You showed me how to structure my thoughts so others could understand them, taught me to ask the right questions, and kept me focused every time I got sidetracked. Last but not least, I thank my parents, who have been with me every step of the way. You saw my potential and made sure I had the tools to develop it and the motivation to apply it. I would also like to thank my friends and family, who always listened when I needed an audience to help describe what I was doing so that others could understand it.

APPROVAL PAGE

This dissertation written by Matthew Carnaghi has been approved by the following committee of the Faculty of The Graduate School at The University of North Carolina at Greensboro.

Committee Chair

Dr. Starobin

Committee Members

Dr. Lageunesse

Dr. Rathnyake

Dr. Ignatova

November 2, 2021

Date of Acceptance by Committee

October 11, 2021

Date of Final Oral Examination

TABLE OF CONTENTS

LIST OF TABLES

LIST OF FIGURES

CHAPTER I: INTRODUCTION

Memory and Processing in the Brain

The initial goal of this project is to bridge the gap between the physiological brain and mathematically-based neuromorphic computing models. Neuromorphic computing is a style of computing that aims to be smarter and more energy-efficient than regular computing by mimicking the behavior of neurons in the brain. Since neuromorphic computing is based on the human brain, it is important to understand how the brain functions. The human brain is comprised of trillions of neurons, with thousands of different neuron cell types. Each neuron contains dendrites which receive signals from other neurons, a cell body that consolidates signals from the dendrites, and an axon which transmits signals to other neurons. The sites where an axon of one neuron connects with the dendrites of other neurons are called synapses (Fig. 1).

Within a synapse, there is a pre-synaptic side on the axon that provides stimuli (usually in the form of the voltage-dependent release of neurotransmitter), and a post-synaptic side on the dendrite that receives stimuli through specialized neurotransmitter receptors. The pre-synaptic and post-synaptic sides of a synapse do not physically touch, creating a gap. When an excitation wave, or action potential (Fig. 2), passes through the axon and reaches the synapse, it is converted from an electrical signal to neurotransmitters, which are able to traverse the gap. Because axons do not have neuroreceptors and dendrites cannot produce neurotransmitters, the synapse can transmit information in only one direction. The strength of a synapse, or the magnitude of its excitatory or inhibitory effect, is determined by the amount of neurotransmitter released per action potential. Neurotransmitters can either potentiate this signal or attenuate the transmission of an action potential.

Figure 1. The Structure of an Idealized Neuron

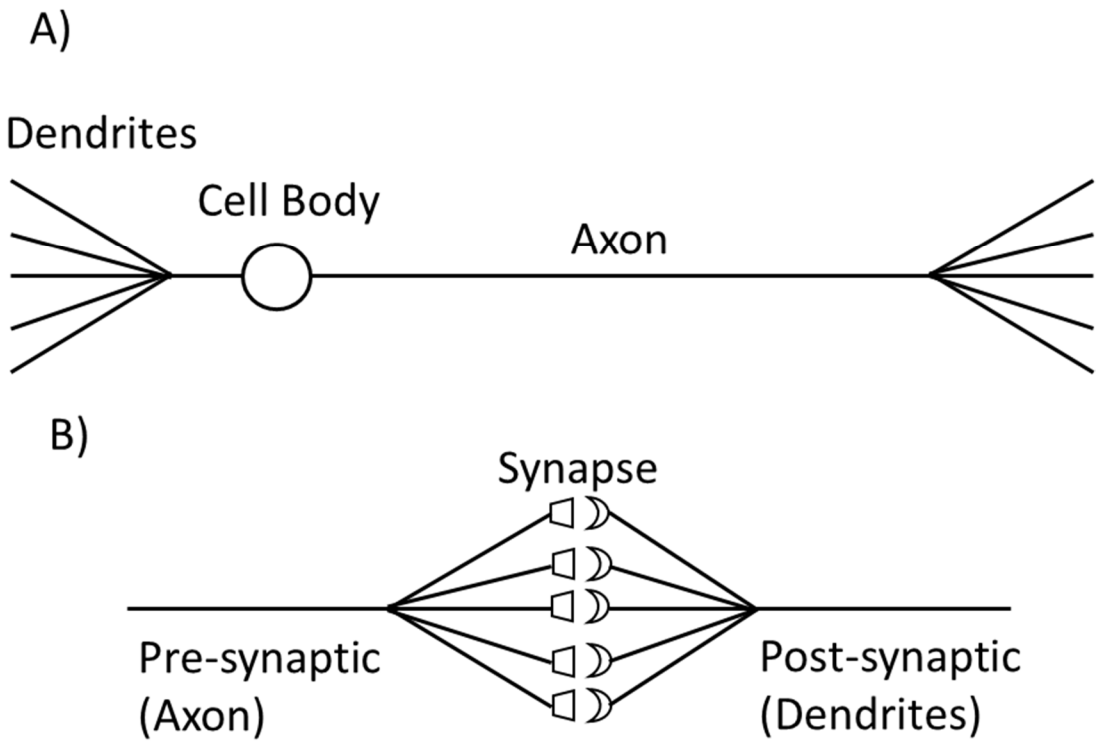

Note A) A single neuron. The region on the left that receives signals from other neurons is called the dendrites, which feed into the cell body from multiple sources (e.g., other neurons). The cell body manages the signals from the dendrites, and if the transmembrane voltage becomes high enough, an action potential propagates through the axon on the right. The axon is able to branch in multiple places, allowing the same signal to be transmitted to multiple target neurons. B) The connection between neurons is called the synapse. The pre-synaptic (axon) and post-synaptic (dendrite) sides interact via a specialized cell-to-cell junction called a synapse, which controls the release and diffusion of neurotransmitters from the pre-synaptic side to their neurotransmitter receptors on the post-synaptic side.

Figure 2. A Typical Action Potential, Modelled in Matlab using Dimensionless Morris-Lecar Equations

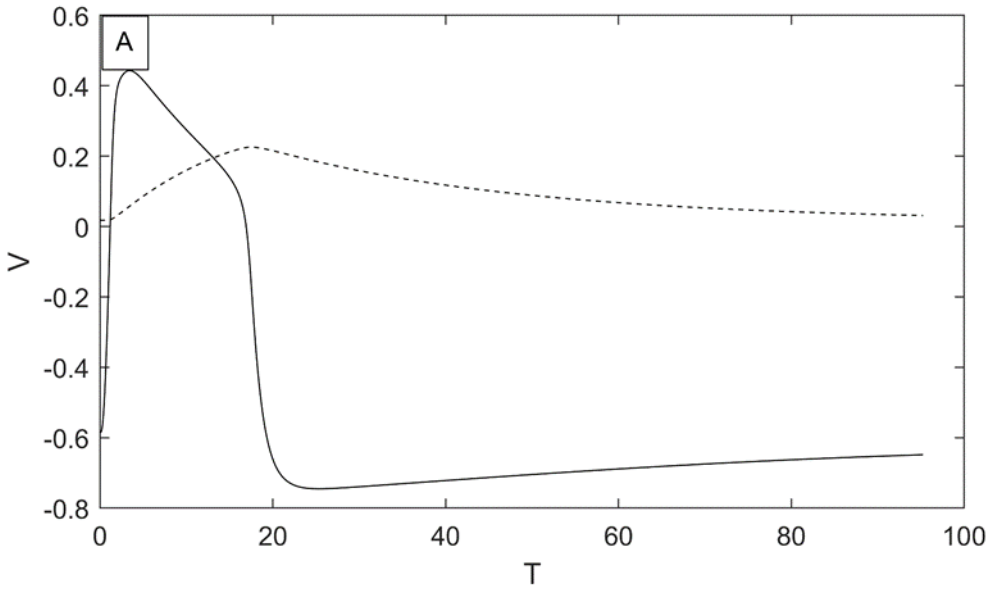

Note The solid line represents the transmembrane voltage of a point along the axon, while the dashed line represents the recovery. The increase in the transmembrane voltage is caused by the influx of sodium ions into the cell, and denotes the wave front. The plateau with slowly decreasing voltage is driven by natural leakage of ions from the neuron, and the sudden decrease in voltage is caused by the outflux of potassium ions leaving the neuron. The potassium gates open when the voltage and recovery values intersect, which also marks the wave back of an action potential. After the potassium ions leave the neuron there is a period of recovery, during which another action potential cannot be formed.

Synaptic strengths change over time through long-term potentiation (LTP) and long-term depression (LTD). LTP is the process of suddenly increasing synaptic strength in response to repeated or strong stimuli, while LTD is the gradual decrease in synaptic strength due to a lack of

stimuli (1,2). It has been determined that the amount of neurotransmitter present affects LTP and LTD, and that the maximum change is double for LTP and half for LTD (3). Memory in the brain is tied to LTP and LTD through the key memory processes of sensitization, habituation, and dishabituation, which are the observable effects of changes in synaptic strengths. Sensitization increases the probability of an action potential by increasing the strength of excitatory synapses (through LTP) and habituation decreases this probability by either increasing the strength of inhibitory synapses (through LTP) or decreasing the strength of excitatory synapses (through LTD) (4,5). Dishabituation is the process through which habituated neurons can become sensitized again, which occurs by either inhibiting the inhibiting/habituating neuron, or by applying a sufficiently large stimulus that triggers LTP and overcomes habituation (6,7).

A common example for demonstrating the role of sensitization and habituation in memory is the startle response in zebrafish (8,9). This is a simple neuronal circuit that contains an auditory sensory neuron, an inhibitory interneuron, and a motor neuron connected to the tail. The sensory neuron excites both the interneuron and the motor neuron, while the interneuron inhibits the motor neuron. When the zebrafish is presented with a loud sound, an action potential is triggered in the sensory neuron, and is transmitted to both the interneuron and the motor neuron. If the sound is unfamiliar, the excitatory strength of the synapse connecting the sensory neuron to the motor neuron is greater than the inhibitory strength of the synapse connecting the interneuron to the motor neuron, and the action potential successfully travels to the tail, causing the zebrafish to move or "startle" (8,9). As the zebrafish is repeatedly presented with the loud sound, the interneuron becomes sensitized through LTP, allowing the inhibitory synapse to overcome the excitatory synapse and habituate the motor neuron. Since the motor neuron does not transmit action potentials, the excitatory synapse undergoes LTD. The startle response demonstrates memory

because as the zebrafish is repeatedly exposed to the loud sound, it becomes familiar with the sound and no longer reacts to it.

Sensitization and habituation can also be tied to several neurological diseases, like post-traumatic stress disorder (PTSD) and dementia (10–12). PTSD can occur after a vivid traumatic event, and stimuli that trigger a memory of that event are met with a strong emotional response (10,11). This is related to memory as the response to fear becomes sensitized, and fear extinction becomes habituated (11). Dementia is characterized as the inability of the aging brain to remember recently-occurring events (12). To compensate for this, the brain increases the number of excitatory synapses (13), which results in a slower speed for processing information (14).

In addition to memory, the brain is also capable of information processing. Processing occurs when there are a large number of connections, and can be structured as shown in Fig. 3. While the most efficient design for information processing would be densely connected neurons spanning long distances (15), this organization is metabolically expensive and costly to maintain. The densely packed structure is also less robust, as long connections are susceptible to damage from interruptions to the metabolic process (15–19). Because of this, the brain maintains an optimization between wiring costs and efficiency (Fig. 3B), resulting in structures called modules (15,16,20).

Figure 3. Different Methods of Organization for Information Processing

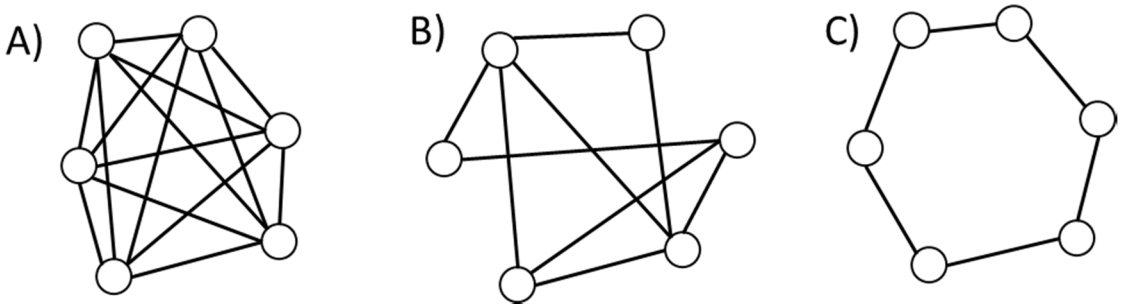

Note A) The structure that optimizes processing efficiency by forming every available connection. The high density of connections maximizes information processing, but also maximizes the total length of axons. As such, this organization is too metabolically expensive. B) The structure that balances processing efficiency and metabolic costs. In this organization neurons that are close together form connections more readily, with long axons reserved for specific connections. This design maintains a high density of connections while significantly reducing the total axonal length, striking a balance between processing efficiency and metabolic costs. C) The structure that optimizes metabolic costs. This organization only allows connections to adjacent cells, minimizing both the axonal lengths and metabolic costs. However, the low connection density also minimizes the processing efficiency.

Modules are regions in brain with high connectivity, defined by a large number of neurons with short connection lengths (Fig.4) (15,16). Because the neurons are clustered together, modules optimize energy cost vs. processing efficiency by reducing the need for long axons. The neurons within a module are categorized as hubs, nodes, and edges based on the density of connections relative to the number of neurons present (Fig. 4). Hubs are neurons that have a high density of connections and are classified as either connector hubs, if they span between modules, or provincial hubs, if they are contained within a single module (15). Nodes are neurons with a moderate density of connections, and edges are neurons with few connections.

Figure 4. An Example of Modules and the Connections Between Them

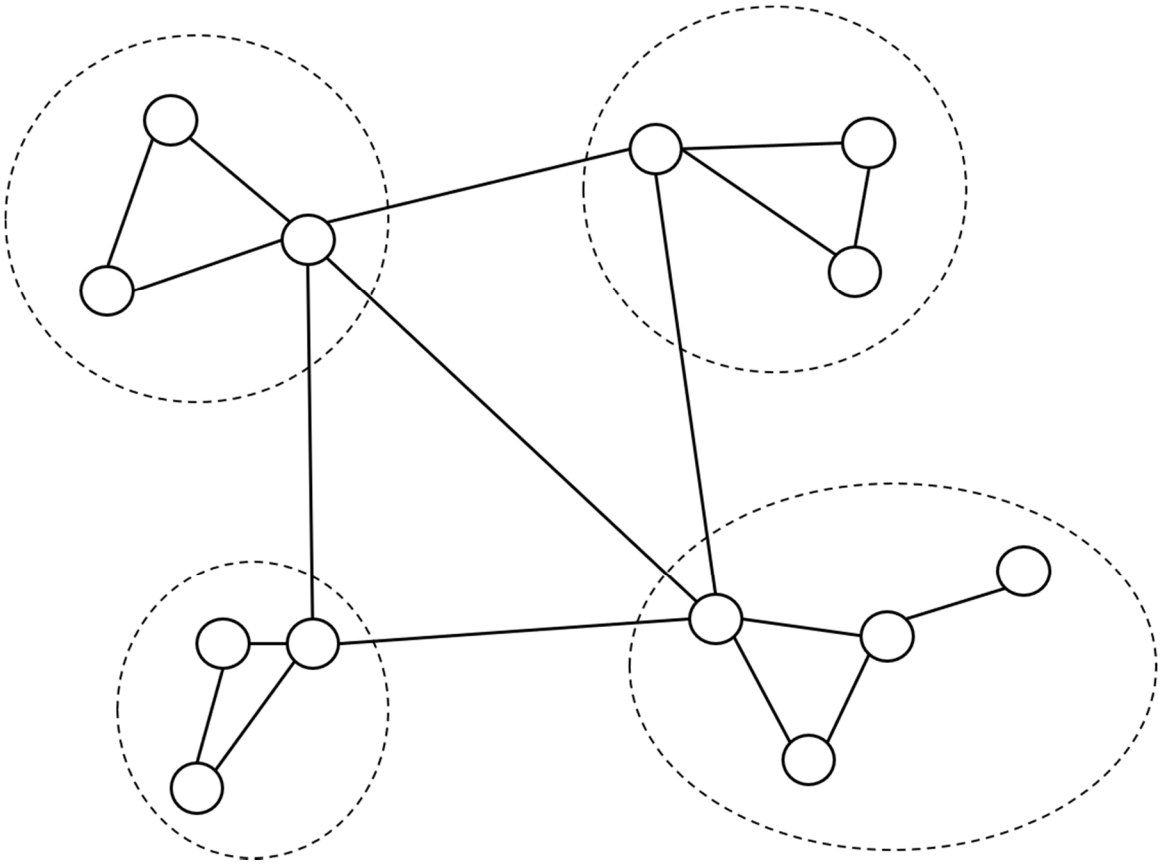

Note Each circled region is its own module, and the connections within each module are noticeably shorter than the connections between modules.

Processing that occurs within a single module is called segregated processing, which handles simple tasks that do not require much thought or need to be handled quickly, such as reacting to a stimulus (15). For example, when treating the zebrafish startle response as a module, the auditory sensory neuron and the motor neuron would act as connector hubs as they extend beyond the module, and the interneuron would serve as either a node or provincial hub (Fig. 5). Based on the purpose of the startle response, the task being processed is determining whether to react to a loud noise. Because the task is simple, the module needs only three neurons, resulting in a minimally structured module. When multiple modules are needed to process a task, it is called

integrated processing. Integrated processing is used for complex tasks, such as solving an equation or answering questions on an IQ test (15). Information is transferred between modules, allowing the task to be performed in parallel. More complicated tasks require a greater number of modules to perform.

Figure 5. An Illustration of the Startle Response in Zebrafish Based on the Descriptions Given in (8,9)

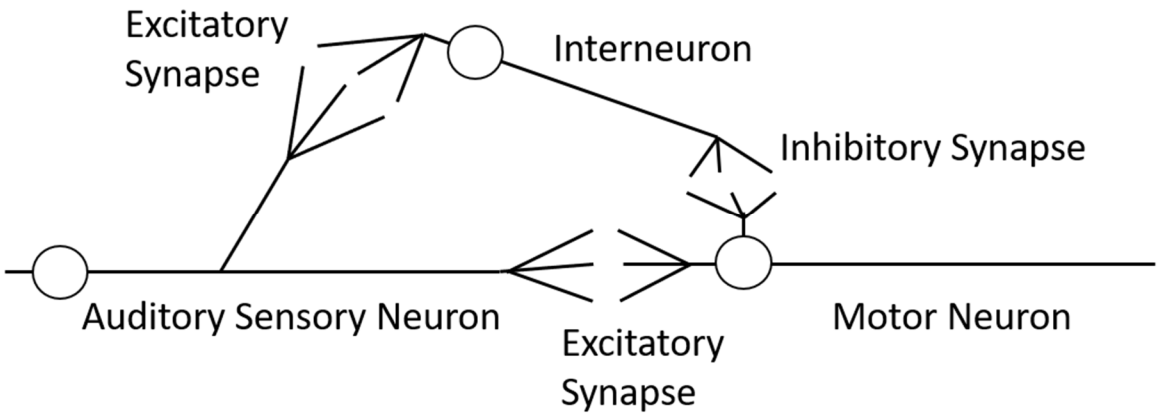

Note When treated as a module, the sensory and motors neurons act as connector hubs since they receive or send information outside of the module. The interneuron can be treated as either a node, because it is only connected to two neurons, or a provincial hub, since it is connected to every other neuron in the module.

To summarize, the brain is capable of both memory and information processing. Memory is controlled by the processes of sensitization, habituation, and dishabituation, which in turn are affected by LTP and LTD. Information processing takes place within modules, which are regions in the brain with short, densely connected neurons. Modules are optimized to balance processing efficiency and metabolic costs, and can act independently for segregated processing or jointly for integrated processing.

Neuromorphic Approaches to Modelling the Brain

Classical computing systems behave exactly as they are programmed to, with minimal ability to learn or to perform tasks independently (21). These systems are fragile, as a single faulty element in a component can render it inoperative. One approach to fix these issues is neuromorphic computing in which computer systems are designed to function like the human brain. Neuromorphic systems are more robust, have a higher level of adaptability, and tend to be more efficient than classical computing systems (22).

The three types of neuromorphic computing systems are memristors, integrate-and-fire equations, and reaction-diffusion equations. Of these three, the reaction-diffusion equations were chosen for this project over memristors and integrate-and-fire equations because the reaction-diffusion equations naturally incorporate delays associated with propagating action potentials. The integrate-and-fire equations require delays to be added manually and memristors do not incorporate delays (23,24). Additionally, the reaction-diffusion equations model the entire neuron, instead of treating the neuron as a single point (Fig. 6). The reaction portion of the equations represents the flow of ions both into and out of the cell, while the diffusion portion covers the movement of ions along the neuron's axon. Because this approach models the entire axon the delays associated with the propagation of excitation waves are inherently present.

Figure 6. A Reaction-Diffusion Representation of the Zebrafish Startle Response Circuit

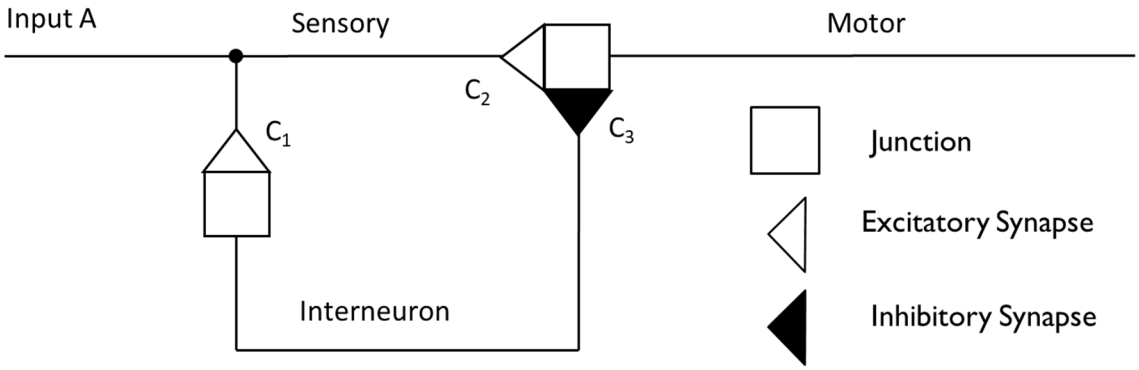

Note This model behaves in the same way as the zebrafish circuit, sending a signal to both the interneuron and motor neuron in response to external stimuli (Input A). Depending on the synaptic strengths ($C_{1\text{-}3}$) the motor neuron can become activated (sensitization) or remain at rest (habituation).

The three main reaction-diffusion equations for neurons are the Hodgkin-Huxley equations, the Morris-Lecar equations, and the Fitzhugh-Nagumo equations. The Hodgkin-Huxley equations are the most detailed and complex, while the Fitzhugh-Nagumo equations are the simplest and easiest to implement. For this work the Morris-Lecar equations were used, as they are capable of complex behavior not seen in the Fitzhugh-Nagumo model (25), yet are more manageable than the Hodgkin-Huxley equations because of the reduced number of variables.

Goals and Objectives

The two major goals of this project are to model the brain functions of both memory and processing using a reaction-diffusion computational model. The hypotheses for both goals are as follows: 1) It is possible to model the brain function of memory using the Reaction-Diffusion Memory Unit (RDMU). The RDMU needs to A) demonstrate sensitization through the activation of a target neuron; B) demonstrate habituation through the inhibition of a target neuron; C) demonstrate dishabituation through the activation of a habituated target neuron. 2) It is possible to model the brain function of information processing using the Reaction-Diffusion Brain Module (BM). Since processing is a vague term, the specific goal is to model single-digit binary addition. To perform this task, the BM needs to A) distinguish between the number of inputs; B) determine the correct output based on the inputs; C) determine the conditions under which single-digit addition can take place.

CHAPTER II: REACTION-DIFFUSION MEMORY UNIT

Background Information

The goal of this section is to model the brain process of memory. The formation of memory has been linked to long-term potentiation (LTP) and long-term depression (LTD), or the lasting increase or decrease of the strength of synaptic connections (1,2). Through LTP and LTD, information is stored, and behavioral patterns can become fixed in the brain. LTP and LTD occurs after a period of learning, which is dominated by sensitization and habituation (2).

Sensitization and habituation are two basic processes in memory that are controlled by the strength of synaptic connection. Sensitization increases the probability that a given stimulus will produce a downstream transmembrane potential by increasing the connectivity of excitatory synapses while habituation decreases the probability of a transmembrane potential by increasing the connectivity of inhibitory synapses (4,26). This has been demonstrated in experiments on the gill withdrawal reflex in *Aplysia californica*, where repeated stimulation cased a prolonged withdrawal of the gill (27,28).

The process of altering behavior based on changes in synaptic connection strengths is known as synaptic plasticity and is considered to be the underlying mechanism of the formation of memory (27,29). So far, the main stream approach to model the formation of memory was based on the threshold models of individual neurons (23,30,31). Nevertheless, these models did not consider physiological reaction-diffusion mechanisms which are responsible for the conduction of excitation in the neuronal environment. A recent effort to incorporate reaction-diffusion effects to quantify changes in the synaptic strength of isolated biological synapses (32) and synaptic-like memristor elements (33) was a step in the right direction. However, it still did not help to elucidate the reaction-diffusion origin of sensitization and habituation.

Another way to account for the spatial distribution of neuronal structures is the introduction of the concept of a meta-neuron. A meta-neuron consists of a relatively small group of several tens of neurons, which may be collectively involved in a particular macroscopic function. Such a structure includes Hodgkin-Huxley axons with added synaptic connections described by a set of gating equations (34). In general, this approach may be considered as an adequate tool to describe large neuronal clusters, yet it entirely ignores the essential structural details which govern the balance between sensitization and habituation needed to process the information by a particular memory unit.

A typical example of sensitization and habituation can be seen in the startle response in zebrafish. The startle circuit is comprised of an auditory sensory neuron, a Mauthner cell (motor neuron) that triggers startle movement, and an inhibitory neuron that prevents familiar stimuli from triggering a startle response (8,9). The auditory neuron connects to both the inhibitory neuron and Mauthner cell with two excitatory synapse regions. The inhibitory neuron also connects to the Mauthner cell with an inhibitory synapse region. As a new incoming stimulus is repeated, the excitatory synapses connecting to the inhibitory neuron strengthen, and inhibitory synapses connecting to the Mauthner cell strengthen as well, resulting in less frequent triggering of the startle response. Although the described above circuit may be useful for explanation of a simple startle response in zebrafish (8), it lacks sufficient complexity to relate to the abrupt disappearance of habituation (dishabituation) which, according to Groves and Thompson dual-process theory that sensitization and habituation are in competition, occurs even if the strength of excitatory synapses in the sensory neuron remains constant (26).

More complex examples of habituation are described in Sokolov's comparator and Ramaswami's negative-image models (6,7). The system for the formation of the model in

Sokolov's approach inhibits the excitatory process for recognized stimuli. When presented with unfamiliar stimuli, this inhibition ceases, resulting in dishabituation. Similarly, dishabituation may also occur in the negative-image model by inhibiting the negative image that negates incoming stimuli.

Based on these examples, a novel method was proposed that uses a reaction-diffusion approach and is capable of quantifying combined effects of sensitization, habituation, and dishabituation by connecting just a few axons with several synapses of adjustable strength. This model incorporates a system of three Morris-Lecar-type neurons (35) linked by four synapses defined by Hebbian synaptic strength rules (36), which will be described later. The circuit is connected to two distinct Morris-Lecar-type input cables to allow a separate stimulation of sensory and inhibitory neurons. This system will be further referred to as the reaction-diffusion memory unit (RDMU) (Fig. 7).

Figure 7. The Structure of the RDMU

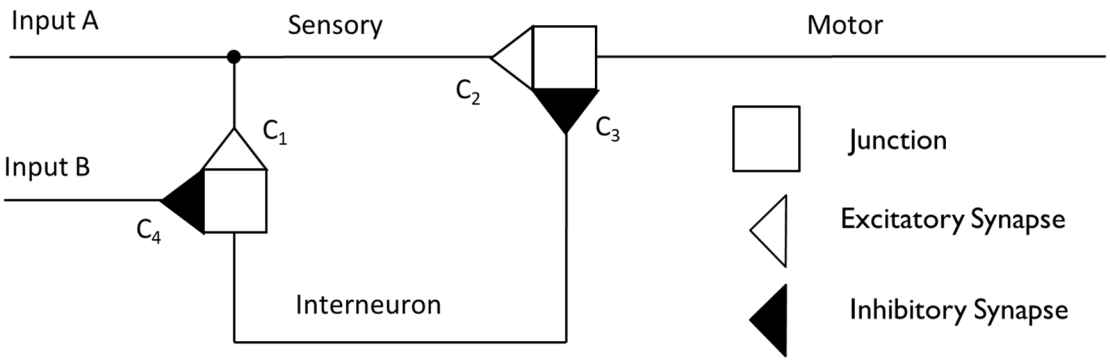

Note Excitatory synapses C_1 and C_2 are shown as empty triangles. Inhibitory synapses C_3 and C_4 are represented by filled-in triangles. Synaptic junctions are denoted by empty squares and the neuronal branching point is marked with an empty circle. The portion of the RDMU between C_1 and C_3 is the interneuron.

Unlike conventional spiking threshold models, which implement integrate-and-fire equations, the reaction-diffusion approach eliminates the need for the use of purely phenomenological temporal delays associated with the propagation of excitation from one neuron to another (37,38). Instead, these delays form naturally because of spatial-temporal evolution of excitation waves under the influence of different rates of cellular membrane polarization and re-polarization processes, various neuronal lengths, and altered strengths of synaptic connections between different neuronal fibers.

Model and Methods

It is possible to illustrate each individual synaptic connection as shown in Fig. 8. To quantify cases with an arbitrary number of such connections, we define a variable *C* as a conglomerate synapse given by the sum in Eq. (1)

$$C = \sum_{i=1}^{n} s_i \tag{1}$$

where excitatory and inhibitory synaptic weights s_i between two specific neurons have positive and negative signs, respectively. The sign of the conglomerate synapse *C* tells whether the net effect of all connection in the bundle is excitatory (+) or inhibitory (-) (Fig. 8).

Figure 8. The Summation of Weights of Individual Synaptic Connections to a Conglomerate Synapse *C*

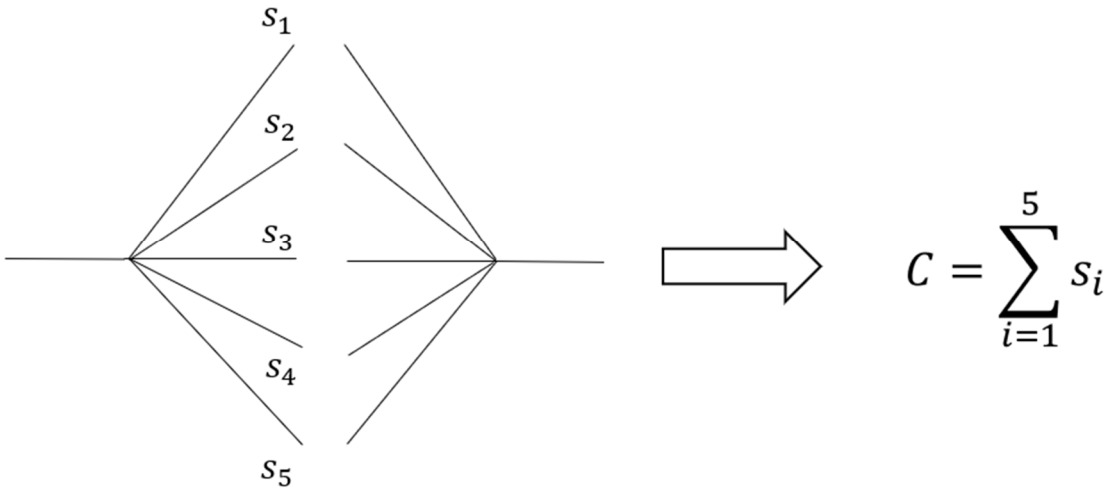

Using synaptic connections determined by Eq. (1), one can link neurons to elucidate the processes of sensitization, habituation, and dishabituation (Fig 7). In this figure, the initial propagation of the transmembrane potential is provided by stimulating inputs A and B. The further evolution of the wave from input A causes sensitization through the passage of excitatory synapse C_2. The wave also propagates to the interneuron through excitatory synapse C_1 and produces habituation via inhibitory synapse C_3. The evolution of the wave from input B causes dishabituation by passing through inhibitory synapse C_4.

The RDMU is studied mathematically using a Morris-Lecar model with incorporated Hebbian conditions at the synaptic junctions, no-flux boundary conditions at the ends of neurons, and additional diffusion terms at the sensory neuron's branching point (35) (Fig. 7). The equations for the Morris-Lecar model are as follows:

$$C_0 \frac{\partial v}{\partial t} = -g_L(v - v_L) - M_\infty g_{Ca}(v - v_{Ca}) - g_K w(v - v_K) + D\frac{\partial^2 v}{\partial t^2} + F(t) \qquad (2)$$

$$\frac{\partial w}{\partial t} = \frac{(W_\infty - w)}{\tau} \qquad (3)$$

$$M_\infty = \frac{1}{2}\left(1 + \tanh\left(\frac{v - v_1}{v_2}\right)\right) \quad (4)$$

$$W_\infty = \frac{1}{2}\left(1 + \tanh\left(\frac{v - v_3}{v_4}\right)\right) \quad (5)$$

$$\tau = \frac{1}{\phi}\operatorname{sech}\left(\frac{v - v_3}{2v_4}\right) \quad (6)$$

$$F(t) = \begin{cases} I, & t \le t_{dur} \\ 0, & t > t_{dur} \end{cases} \quad (7)$$

where I and t_{dur} are the amplitude of the external current (stimulus) and its duration, respectively. Variables v and w represent the transmembrane voltage and dimensionless gating variable corresponding to the inhibitory response of the potassium channels. Parameters v_L, v_{Ca}, and v_K are equilibrium potentials for leakage, calcium, and potassium currents, respectively. Factors M_∞ and W_∞ are dimensionless constants which are determined by regulating voltages v_1, v_2, v_3, and v_4 (39).

By introducing specific time and spatial scales, one can define a set of dimensionless variables as follows:

$$v^* = \frac{v}{v_{Ca}}, v_i^* = \frac{v_i}{v_{Ca}}, i = L, K, Ca, 1,2,3,4 \quad (8)$$

$$t^* = t\frac{g_{Ca}}{C_0} \quad (9)$$

$$x^* = \frac{x}{L_0} \quad (10)$$

$$L_D = \sqrt{\frac{D}{g_{Ca}}} \quad (11)$$

$$g_i^* = \frac{g_i}{g_{Ca}}, i = L, K, Ca \quad (12)$$

$$\phi^* = \phi\frac{C_0}{g_{Ca}} \quad (13)$$

Here v^*, t^*, and x^* are dimensionless variables for transmembrane potential, time and spatial variables. Parameters g_L^* and g_K^* refer to dimensionless leakage and potassium conductance, respectively. Parameter g_{Ca}^*, which determines dimensionless calcium conductance, is equal to one. The value of L_D corresponds to the diffusion length. The value of L_0 is the length of the main section of the RDMU, which is equal to the sum of the lengths of the sensory and motor neurons. The scales are given as follows: C_0 = 10μF, v_{Ca} = 100mV, D = 1μS·cm^2, g_{Ca} = 10mS, and L_0 = 1mm.

For simplicity, dimensionless variables will further be referred to as v, w, t, x, g_K, v_K, etc., continuing with dimensionless Morris-Lecar equations in the following way:

$$\frac{\partial v}{\partial t} = F(t) - g_L(v - v_L) - M_\infty(v - v_{Ca}) - g_K w(v - v_K) + \left(\frac{L_D}{L_0}\right)^2 \frac{\partial^2 v}{\partial x^2} \tag{14}$$

$$\frac{\partial w}{\partial t} = \frac{(W_\infty - w)}{\tau} \tag{15}$$

$$M_\infty = \frac{1}{2}\left(1 + \tanh\left(\frac{v - v_1}{v_2}\right)\right) \tag{16}$$

$$W_\infty = \frac{1}{2}\left(1 + \tanh\left(\frac{v - v_3}{v_4}\right)\right) \tag{17}$$

$$\tau = \frac{1}{\phi}\operatorname{sech}\left(\frac{v - v_3}{2v_4}\right) \tag{18}$$

Table 1 summarizes the model dimensionless parameters which, unless otherwise stated, were used in all numerical experiments. These values are based on the dimensional values from (39).

Table 1. The Dimensionless Parameters Used to Solve Model Eqs. (14)-(22)

ϕ	g_{Ca}	g_K	g_L	v_{Ca}	v_K	v_L	v_1	v_2	v_3	v_4	I	v_0	w_0	v^{thr}
.017	1	1.8	.45	1	-.84	-.6	-.012	.18	.02	.30	1	-.58	.0177	-.225

A set of boundary conditions for Eqs. (14-18) includes no-flux conditions at the ends of neurons (Eq. (19)), and Hebbian links between the pre- and post-synaptic values of transmembrane potential at each of the RDMU synapses (Eq. (20)) (36).

$$\frac{\partial v}{\partial x} = 0 \tag{19}$$

$$v_{A,post} - v_0 = C_2\left(v_{A,pre} - v_0\right) + C_3\left(v_{B,pre} - v_0\right) \tag{20A}$$

$$v_{B,post} - v_0 = C_1\left(v_{A,pre} - v_0\right) + C_4\left(v_{B,pre} - v_0\right) \tag{20B}$$

Here C_i, $v_{i,pre}$, $v_{i,post}$, and v_0 are synaptic strengths, pre- and post-synaptic potentials of the i^{th} synapse and resting value of the transmembrane potentials, respectively. The first of Eq. (20) describes the cumulative post-synaptic action of adjacent excitatory and inhibitory synapses C_2 and C_3, located at the beginning of the motor neuron. The second part describes the cumulative post-synaptic action of adjacent excitatory and inhibitory synapses C_1 and C_4, located at the beginning of the interneuron. The resting transmembrane potential, v_0, as well as the resting value of the recovery variable, w_0, are determined by the intersection of null-clines of the system of Eqs. (14) and (15). The null-clines also define the excitation threshold, v^{thr}, as shown in Fig. 9.

Figure 9. The Phase Portrait for the Morris-Lecar Model

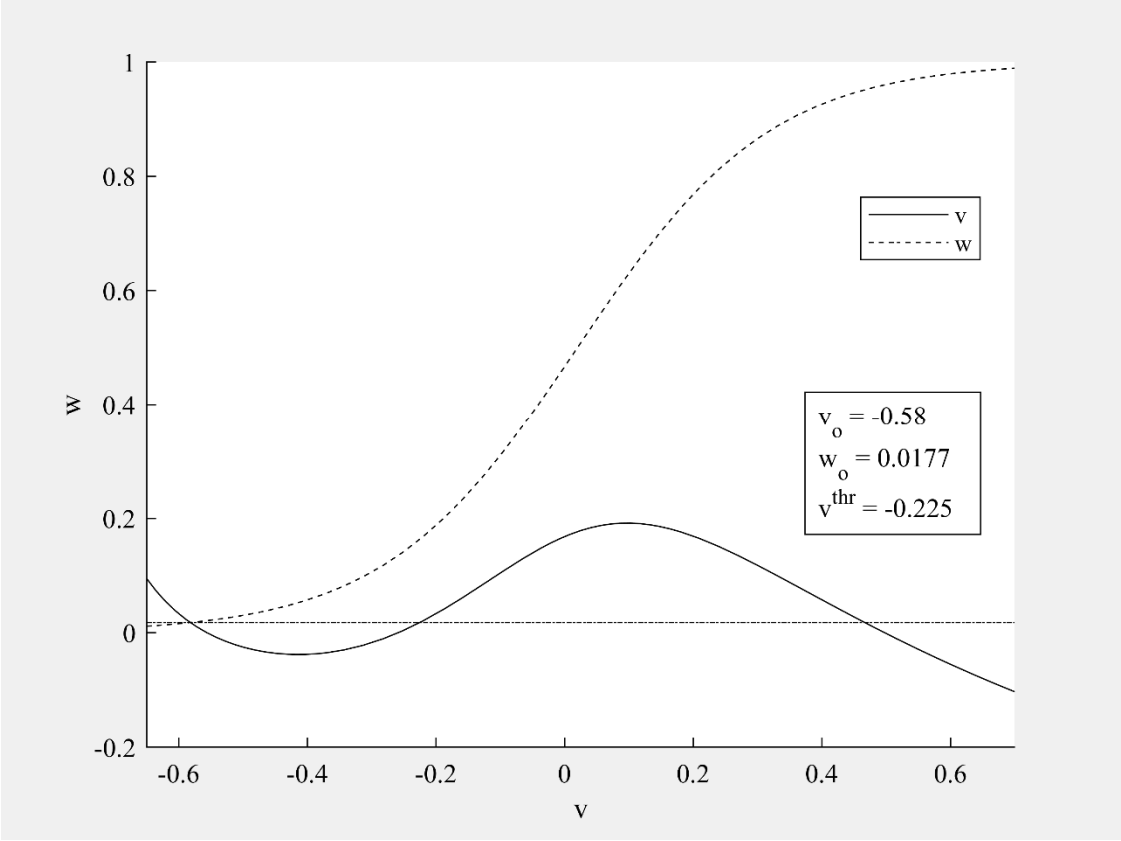

Note The solid line is the null-cline for v and the dashed line is the nullcline for w. The equilibrium values for v and w occur at the intersection of null-clines. The horizontal dot-dashed line has a value of w_0 for all v, and is used to find v^{thr}, which is the second intersection of v and w_0.

To complete the formulation of synaptic conditions one needs an additional boundary condition to warrant that each synapse acts as a unidirectional gate which prevents the backwards flow of transmembrane potentials. This condition is defined by Eq. (21):

$$\left.\frac{\partial v}{\partial x}\right|_{x=x^-} = 0 \tag{21}$$

Here x^- is upstream with respect to the direction of the synaptic current.

Finally, the branching point located at the end of input A, where the sensory axon diverges (Fig. 7), is analyzed. At this point one needs to modify Eq. (14) and consider two diffusion terms

and account for cumulative two-dimensional effects comprised of two one-dimensional diffusion processes in the first (x) and the second (y) neuron branches, respectively:

$$\frac{\partial v}{\partial t} = F(t) - g_L(v - v_L) - M_\infty(v - v_{Ca}) \\ -g_K w(v - v_K) + \left(\frac{L_D}{L_0}\right)^2 \left(\frac{\partial^2 v}{\partial x^2} + \frac{\partial^2 v}{\partial y^2}\right) \quad (22)$$

The rationale for considering a linear steady-state Hebbian rule (Eq. (20)) is based upon the observation that behavioral and, to some extent, cognitive memories are associated with neural oscillations withing theta and partial gamma ranges below 20 Hz (40,41). Under these conditions one can consider only isolated stimulating currents (Eq. (7)) applied to the sensory neuron shown in Fig. 7. Indeed, the transmembrane potentials induced by neuronal spikes in the hippocampus are on average 1-3ms in duration (42) and the intervals between successive spikes at frequencies below 20Hz are greater than 50ms. Therefore, the temporal evolution of the transmembrane potential resulted from a previous neuronal spike becomes completed well before the initiation of the next spiking activity. Accordingly, propagation of the transmembrane potentials in the RDMU branches evolves into transmission of the steady-state solitary pulses. Finally, since the propagation of transmembrane potentials is steady-state, a temporal derivative term in the Hebbian rule (36) can be omitted and the resulting steady-state Hebbian links can be expressed as linear algebraic relations described by Eq. (20).

The system of Eqs. (14)-(22) was solved numerically using an explicit finite difference method (See appendix of (43)). The dimensionless time and space steps were $\Delta t = 2.5\times10^{-5}$ and $\Delta x = 0.1$ for all experiments, respectively. Parameter $\left(\frac{L_D}{L_0}\right)^2$ in Eqs. (14) and (22) was set to 0.01.

Unless stated otherwise, the sensory neuron and both inputs spanned 25 spatial intervals each, while the motor neuron and interneuron individually consisted of 50 spatial intervals (Fig.

10). At the initial time $t = 0$ an external stimulus I of amplitude one was applied for a duration of $5\times10^4\Delta t$ to nodes one through fifteen located at the beginning of inputs A and B.

Figure 10. The Diagram Which Depicts the Spatial Scales of the RDMU

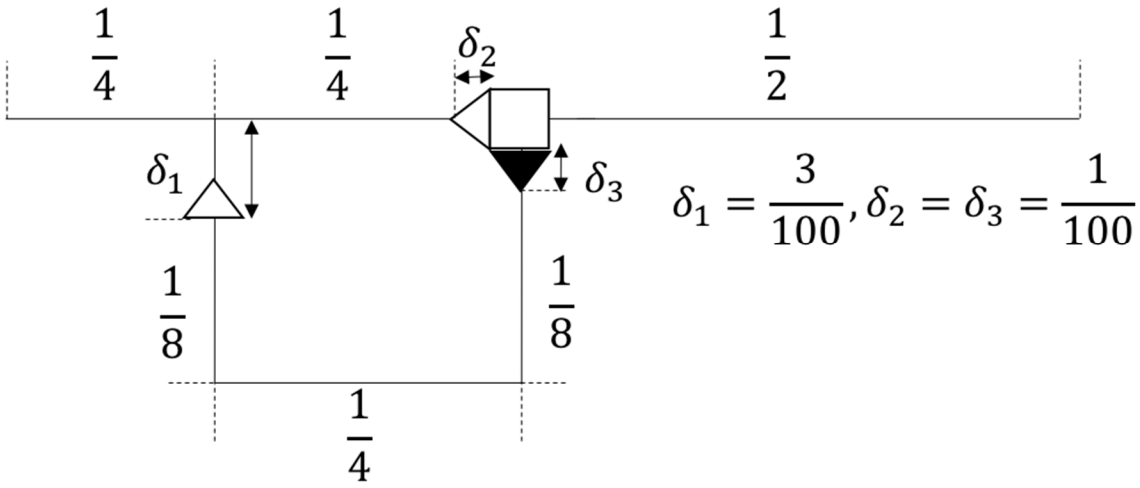

Taking into consideration that the speed of transmembrane potentials in the brain is on average greater than 10m/s, parameters in Table 1 were set to reflect that the width of the excitation wave is much longer than a one millimeter total length of the sensory and motor neurons (44,45). Typical spatial and temporal evolutions of such waves are depicted in Fig. 11.

Figure 11. Transmembrane Potential *v* and Gating Variable *w* as Functions of Spatial Variable *x*

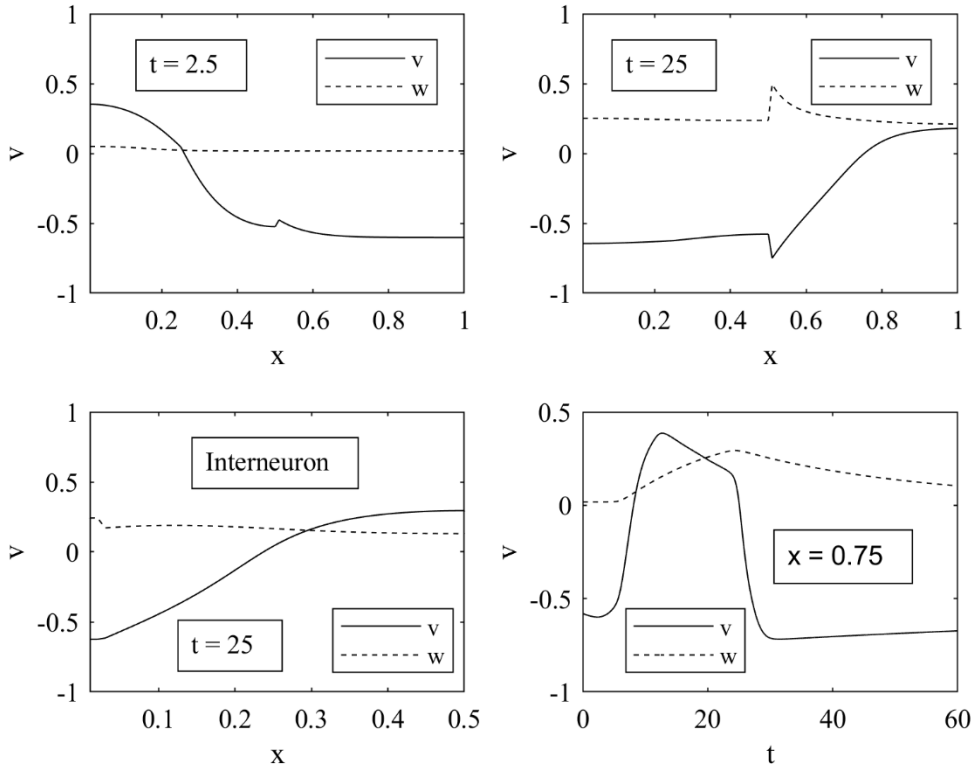

Note Upper panels show a spatial evolution of the excitation pulse in the sensory and motor neurons in the interval of time between 2.5 and 25. Lower left panel shows progression of the excitation pulse in the interneuron at time 25. Lower right panel illustrates temporal evolution of excitation at $x = 0.75$. Parameters C_1, C_2, and C_3 are equal to 1, 1.8, and -0.2, respectively, for ideal propagation through all regions.

The propagation of solitary pulses originated by identical input stimuli, I, applied to both inputs of the RDMU was studied. A series of numerical simulations has been performed to evaluate the RDMU's ability to reproduce the processes of sensitization, habituation, and dishabituation. Depending on the values of synaptic strengths C_1, C_2, C_3, and C_4, the input stimuli propagated to

the motor neuron and originated either sub-threshold or over-threshold responses, thus signifying the initiation of processes of sensitization, habituation, and dishabituation.

The synaptic strength boundary between sensitization and habituation (BSH) was computed iteratively with the value of C_4 fixed at zero. At fixed values of C_2 the value of C_3 was incrementally adjusted until regimes changed from sensitization to habituation, preventing the propagation of the over-threshold stimulus in the motor neuron. After that, the values of C_2 were increased by a set of sufficiently small increments and the process was repeated until values of C_2 were equal to 1.5 of values of $|C_3|$ exceeded 5, beyond which the BSH and BHDH curves become linearly proportional. The boundary between habituation and dishabituation (BHDH) was calculated in the same manner at different values of C_4.

Results and Discussion

It was determined whether the system was in sensitization, habituation, or dishabituation by comparing the maximum transmembrane potential to a threshold potential shown in Fig. 9. The threshold potential was increased by 20% to account for wave propagation decay due to diffusion. BSH and BHDH curves were determined depending on whether the maximum transmembrane potential exceeded the modified threshold or remained below it. It was found that the difference between BSH and BHDH curves measured at 10 Δx from the end of the motor neuron and further away (30 Δx) did not exceed 5% and 16% at low and high values of C_3, respectively. We chose to measure the magnitude of the transmembrane potentials closer to the end of the motor neuron at 10 Δx.

One of the main parts of the numerical simulations was focused on investigating the influence of the relaxation parameter ϕ and the potassium conductance and leakage conductance on the dynamics of excitation pulses in the RDMU. As expected, it was found that the magnitude

of ϕ significantly affected the rate of relaxation of recovery variable w, and therefore invoked considerable changes in the width and speed of the excitation pulse. Potassium and leakage conductances also contributed to changes of the width of the pulse in a noticeable way. Figure 12 demonstrates various shaped of excitation pulses for different parameters ϕ, g_K, and g_L. One can observe that smaller values of ϕ cause prolongation of pulses. Similar changes occur due to the decrease of either g_K or g_L.

Figure 12. Various Transmembrane Potentials for Different Sets of Parameters

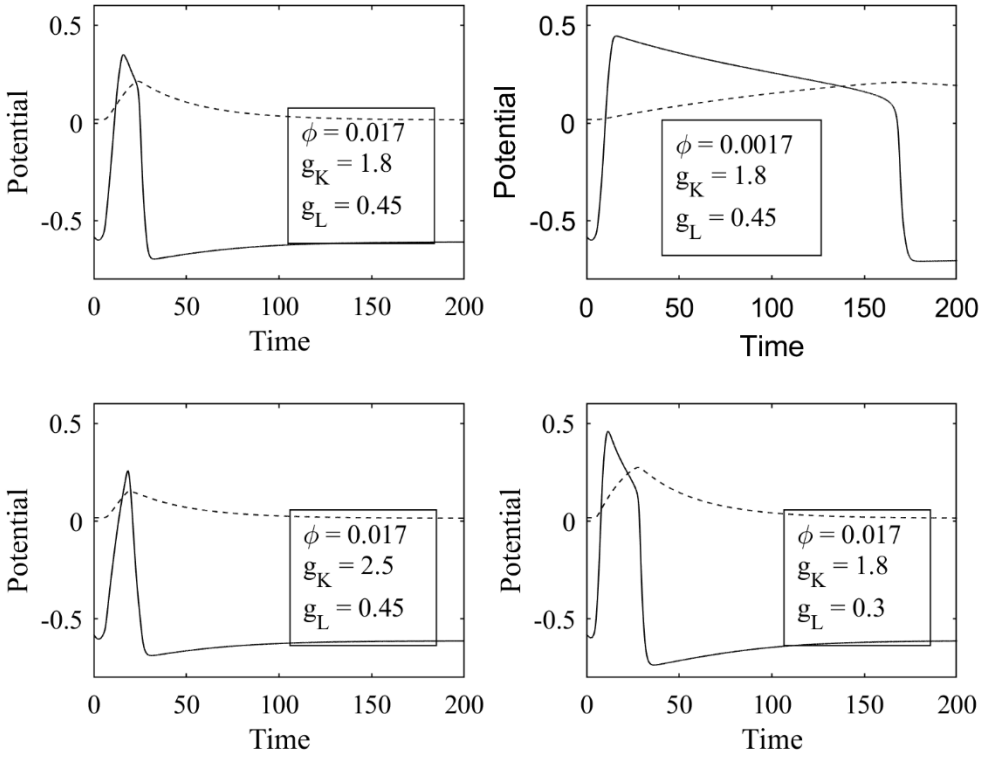

Note The top left panel depicts the transmembrane potential for the parameters in Table 1, while the tip right, bottom left, and bottom right show the transmembrane potentials for decreased ϕ, increased g_K, and decreased g_L, respectively.

A series of numerical simulations was performed to study the edge between sensitization and habituation processes in the RDMU, where the propagation of excitation waves is depicted in Fig. 12. As shown in Fig. 13 the BSH can be adequately described by Eq. (23) (See also Table 2).

$$C_3 = aC_2^b + c, b > 1 \quad (23)$$

Table 2. Constants a, b, and c for Curves Depicted in Figs. 13 and 14

ϕ, g_K, g_L, C_1	*a*	*b*	*c*	Figure/curve shape
0.0017, 2.5, 0.45, 0.8	-3.81	2.76	1.59	14, filled circle
0.0017, 1.8, 0.45, 0.8	-3.37	3.14	1.06	14, filled square
0.0017, 1.8, 0.3, 0.8	-3.39	3.60	0.33	13, filled square
0.017, 1.8, 0.3, 0.8	-3.36	3.47	0.59	13, open square
0.0017, 1.8, 0.3, 0.6	-21.11	5.50	0.57	13, filled diamond
0.017, 1.8, 0.3, 0.6	-18.08	4.08	2.10	13, open diamond

Note The values of these constants are determined from Eq. (23) using linear regression.

Figure 13. Sensitization-Habituation Boundaries Depicted as Dependences of C_3 on C_2 for Different Values of ϕ and g_L (g_K = 1.8)

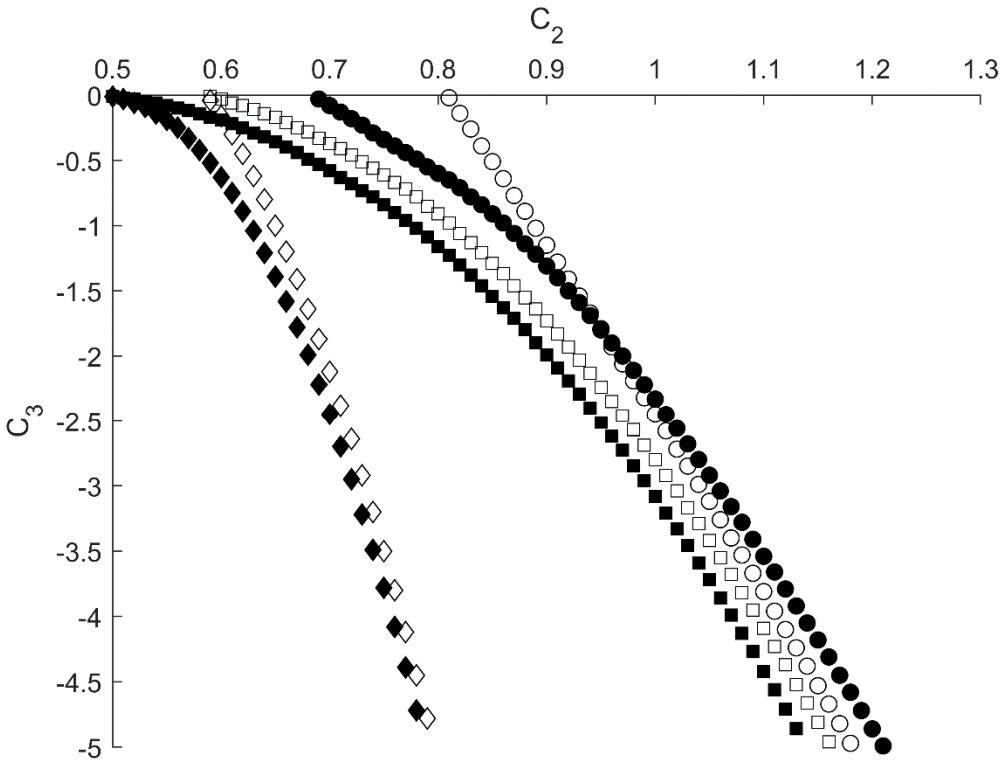

Note Open and filled shapes correspond to ϕ = 0.017 and ϕ = 0.0017, respectively. Parameter C_1 is equal to 0.8 for all curves except open and filled diamonds, where C_1 = 0.6. Circles correspond to g_L = 0.45 while diamonds and squares relate to g_L = 0.3. Other parameters are fixed at values shown in Table 1.

It should be noted that shorter (slower) pulses with higher values of ϕ correspond to lower absolute values of the inhibitory synaptic strength $|C_3|$, thus indicating that it is easier to counter play an excitatory action of the synapse C_2 for higher magnitudes of relaxation parameter ϕ. Alternatively, it was found that a decrease of leakage conductance g_L resulted in an opposite shift of BSH towards higher values of $|C_3|$ associated with greater thresholds required to inhibit the RDMU at any given strength of C_2 (Fig. 13).

As shown in Fig. 7, the excitatory synapse C_1 plays a role as some type of a gate which regulates the flow of transmembrane potentials between the sensory and interneuron branches of the RDMU. Specifically, it varies the transmembrane potential's diffusion flux, and therefore controls the amplitude of the excitation pulse which propagates through the inter-neuronal branch of the RDMU.

At lower values of C_1, as well as in case of lesser g_L, a significant shift of the BSH towards high values of $|C_3|$ is again observed (Fig. 13). Specifically, at $C_1 = 0.6$ and $C_2 = 0.65$ the value of $|C_3|$ required for the suppression of a pulse in the motor neuron was more than three times greater than a corresponding value of $|C_3|$ necessary for the suppression of a similar pule at $C_1 = 0.8$. It should be noted that all BSH curves depicted in Fig. 13 are in agreement with approximation (23), since values of b are greater than one (Table 2). However, when the relaxation parameter ϕ and potassium conductance g_K increase simultaneously the BSH curves turn to nearly directly proportional changes between inhibitory and excitatory synaptic strengths C_2 and C_3 (Fig. 14).

Figure 14. Sensitization-Habituation Boundaries Depicted as Dependences of C_3 on C_2 for Different Values of ϕ and g_K (g_L = 0.45)

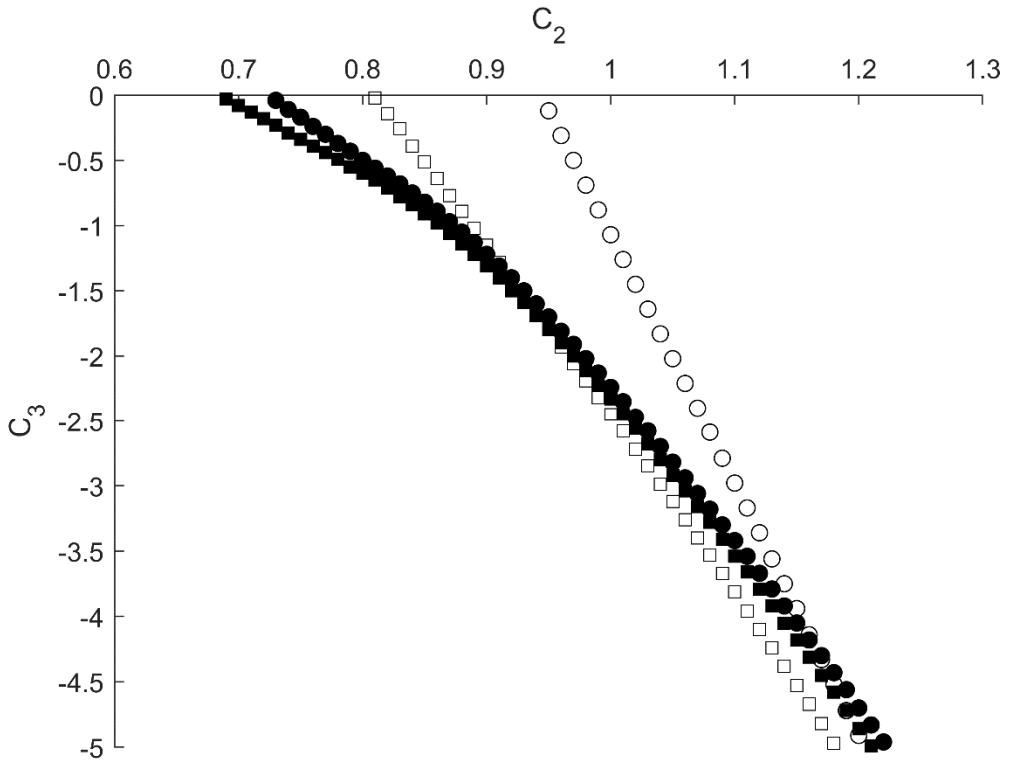

Note Open and filled shapes correspond to ϕ = 0.017 and ϕ = 0.0017, respectively. Circles and squares correspond to g_K = 2.5 and g_K = 1.8, respectively. Other parameters are fixed at values shown in Table 1.

It has been demonstrated above that the propagation of excitation waves from the sensory to motor neuron may significantly depend on both the strengths of the excitatory synapses C_1 and C_2, as well as on the influence of the inhibitory interneuron synaptic connection C_3.

It was also found that the lengths of the RDMU neurons can be additional important contributors into the balance between habituation and sensitization. Accordingly, the larger ratio of the interneuron's length to the total length of the sensory and motor neurons results in a more

significant shift of the BSH curve to the left, making it more difficult to inhibit the RDMU even at smaller values of C_2 (Fig. 15).

Figure 15. Sensitization-Habituation Boundaries Depicted as Dependences of C_3 on C_2 for Different Interneuron Lengths

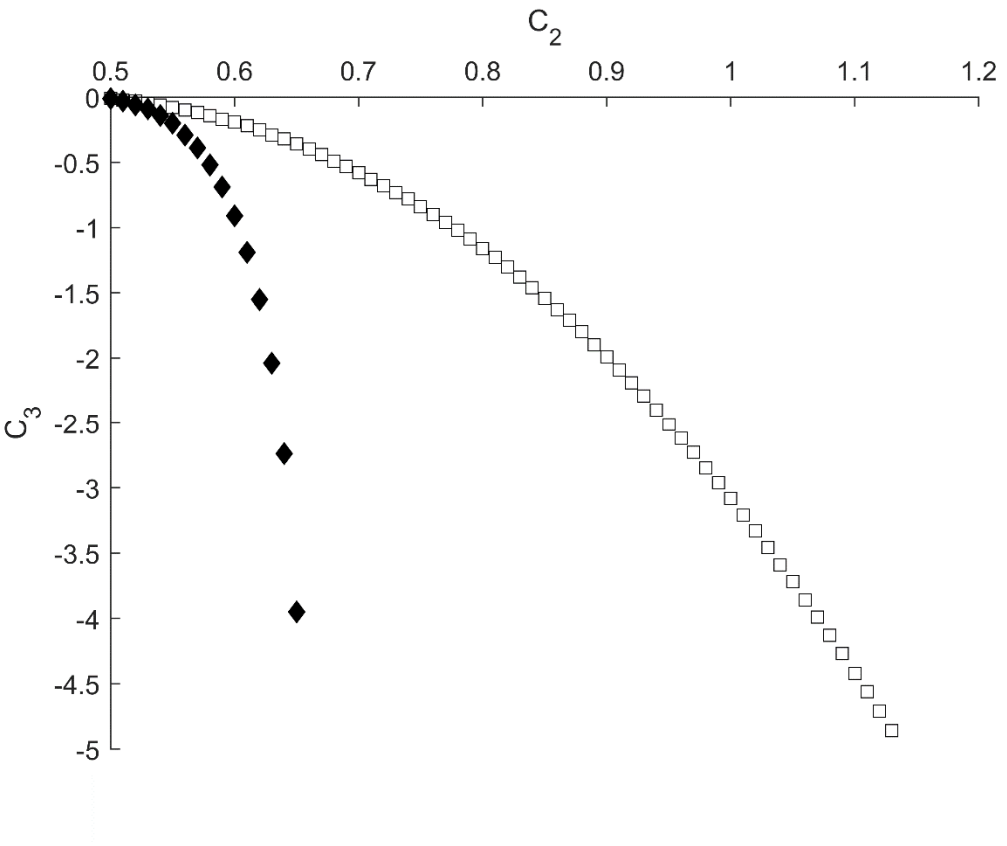

Note Black diamonds denote interneurons with length 0.625 while squares relate to interneurons with length 0.5. Parameters ϕ and g_L are equal to 0.0017 and 0.3, respectively. Other parameters are fixed at values shown in Table 1.

To calculate the BHDH curves, two stimuli were applied through inputs A and B. As shown in Fig. 7, input A connects directly to the interneuron through inhibitory synapse C_4. In this manner, C_4 affects the BHDH curves by decreasing the responsiveness of the interneuron.

It was found that increasing the strength of C_4 resulted in a shift of BHDH curves towards smaller values of C_2, thus reflecting the dishabituation of the motor neuron. This effect is more

pronounced for lower values of g_L, where the shift in C_2 is greater, and the slopes of the BHDH curves are consistently shallower (Fig. 16).

Figure 16. Habituation-Dishabituation Boundaries Depicted as Dependences of C_3 on C_2 for Different Values of C_4

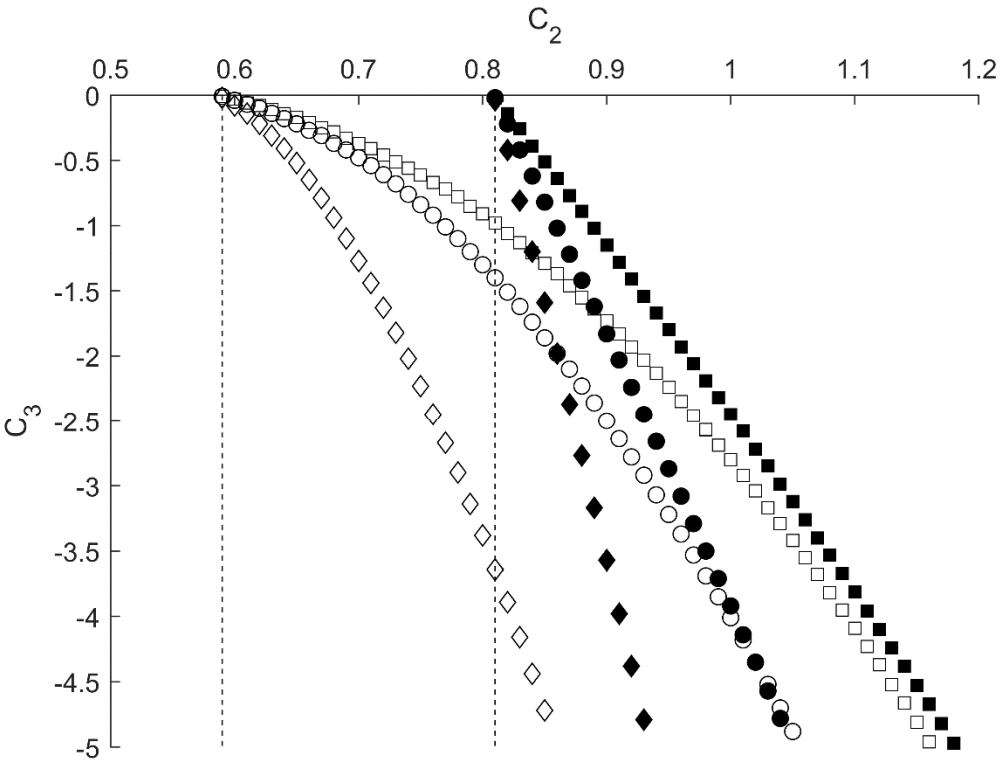

Note Filled shapes represent g_L equal to 0.45 while empty shapes represent g_L equal to 0.3. Squares, circles, and diamonds stand for C_4 equal to 0, 0.05, and 0.15, respectively. Dashed lines correspond to C_4 equal to 0.225. Other parameters are fixed at values shown in Table 1.

As the strength of C_4 further increases, the BHDH curves continue to shift to the left with steeper slopes, until the value of C_4 is approximately 0.225, where the BHDH curves become vertical, as shown by the dashed lines (Fig. 16). Beyond this value, waves in the interneuron are unable to propagate to inhibitory synapse C_3, resulting in complete dishabituation.

Using a novel approach, variations in the BSH dependences were studied in response to changes of parameters of the reaction-diffusion model with Hebbian type synaptic junctions between neurons. It was found that longer transmembrane potential waves (lower g_L), which propagate in the motor neuron, caused the BSH curves to shift towards sensitization. On the contrary, shorter waves (greater g_K) triggered the opposite shift of the BSH curves towards habituation. Also, it was observed that synaptic strength C_1 is another important parameter which has a significant effect on the positioning of BSH.

The value of C_1 directly affects the transmembrane potential flux into the interneuron, thus changing its inhibitory influence on the RDMU. Specifically, it was found that different values of C_1 either substantially reduced or increased the effectiveness of the inhibitory synapse C_3, resulting in a state of the RDMU that is either significantly harder or easier to habituate. In addition to excitatory synapse C_1, inhibitory synapse C_4 also influences the RDMU through changing conditions for dishabituation. Indeed, just a small increase in C_4 produces a notable shift in the BHDH curves towards lower values of excitatory strength in the synapse C_2.

There are two possible approaches for incorporating dishabituation in the RDMU. These two approaches can be derived from the existing concepts of superimposition of sensitization and reversal of habituation described in (46). The first approach is to increase the responsiveness of the motor neuron through an additional strong stimulus, which can be accomplished by adding an additional sensory neuron. In contrast, the second approach is to inhibit the interneuron that causes habituation. While the first approach results in the intertwining of sensitization and dishabituation, since the two processes share the same mechanism, the second one allows sensitization and dishabituation to be further distinguished.

There has been much debate about whether sensitization and dishabituation can be dissociated (46–50). Once again, based on specific experimental procedures, these two processes could either occur through the same mechanisms (47,48) or could have differing ones (46,49,50). The classic dishabituation described in (26) could be an example of superimposed sensitization, where dishabituation and sensitization both result from direct stimulation to the habituated neuron. However, a more recent revision of this work emphasizes the reversal of habituation as another form of dishabituation (5), which was chosen for the RDMU utilizing additional input B (Fig. 7).

CHAPTER III: BRAIN MODULE

Background Information

The goal of this section is to model processing in the brain. Since processing can range from visual recognition, language, cognitive control, emotion, and social cognition (16), this project uses the specific task of single-digit binary addition. Development of novel principles of information processing has generated a significant body of scholarly work and allowed researchers to introduce a unique idea of "unconventional" neuromorphic reaction-diffusion computing systems (51). However, understanding of reaction-diffusion mechanisms of processing of information in the human brain remains a challenging research frontier. Recently it has been shown that reaction-diffusion mechanisms are indeed essential for the functioning of brain memory circuits capable of sensitization and habituation (43). Although these novel concepts allowed for the modeling and quantification of some basic functions of memory, it was not clear if they were suitable for modeling even basic signal processing tasks such as binary operations.

Signal processing in the brain occurs in various neuronal circuits with a sufficiently great number of synaptic junctions and adequate lengths of neurons connecting corresponding synapses. Such conglomerates of neuronal circuits are known as brain modules (BMs), and contain parts with high neuronal connectivity that can extend information to other modules (15), (16). The signal processing performance in BMs is greatly influenced by their structure and dimensions. While longer axons may improve processing performance by connecting distant modules, they are metabolically expensive and more likely to incur damage associated with interruptions in the significant caloric uptake needed for neural maintenance (17). Therefore, neurons with longer axon lengths are more susceptible to diseases caused by disruptions of the metabolic process (15,16,18), (19). As such, the focus will be on modeling simple binary signal operations which can be

performed within a single BM with a minimal composition of synapses connected by shortest straight neuronal fibers (Fig. 17).

To perform binary signal operations, a particular BM needs to be able to both transmit and combine multiple incoming signals. For example, if the BM just transmits the signals without combining them together, it may function as a neuronal circuit capable of modelling the memory related processes of habituation and sensitization in response to external stimuli (43). However, such a BM would be unsuitable for computational operations due to the absence of multiple input signals. To address this deficiency, a BM with a pair of inputs and a pair of outputs interconnected by a single inhibitory interneuron (shown in Fig. 17) was investigated. In this way such a minimally structured BM can transmit input signals one by one or combine them together if the signals are present simultaneously.

Figure 17. The layouts of the brain modules

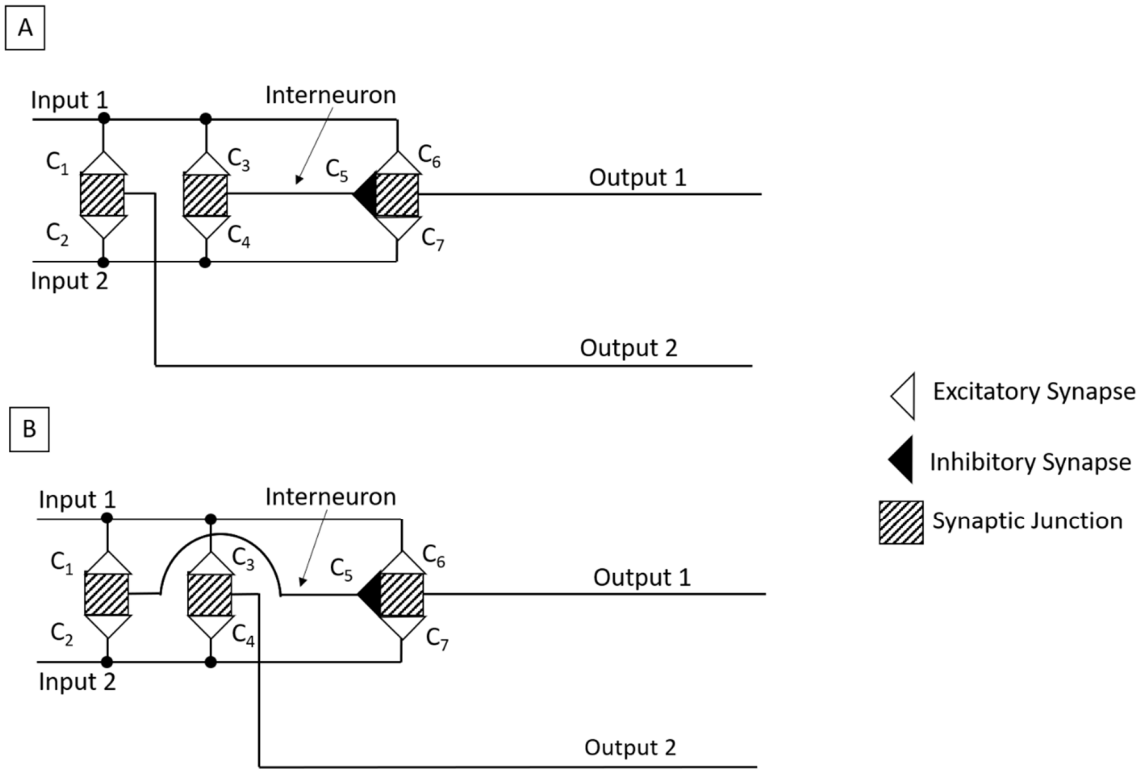

Note A) The BMA is a brain module with shorter interneuron and longer Output 2 neuron. B) The BMB is a brain module with longer interneuron and shorter Output 2 neuron. Signals travel from left to right.

This section examines two types of BM layouts with reduced (Fig. 17, BMA) and prolonged (Fig. 17, BMB) lengths of the interneuron to ascertain if the neuron's dimensions and the order of their connections in the BM affect its capability to process input signals. Specifically, it elucidates a process of combining a pair of synchronous input signals and introduce it as a model of a single-digit binary addition which is essential for signal processing in the BM. Neuronal signals are modelled as propagating reaction-diffusion waves, and the neuronal reaction-diffusion parameters and the values of synaptic strengths needed to minimize the time to perform this single-digit binary operation are determined.

Model and Methods

To examine the propagation of excitation waves in the BM the dimensionless system of Morris-Lecar reaction-diffusion equations are used for the neurons (35) and Hebbian synaptic equations for the synapses (36,43). While modeling of reaction-diffusion processes in the BM is compatible with any reaction-diffusion equations, the Morris-Lecar equations were specifically chosen as they can exhibit complex behaviors like bursting, which simpler models like the Fitzhugh-Nagumo equations are unable to produce (25). Moreover, the Morris-Lecar equations have fewer parameters than the Hodgkin-Huxley equations, allowing them to be implemented in computations more readily. As in chapter 2, applying the Morris-Lecar approach gives the following system of governing equations in dimensionless form

$$\frac{\partial v}{\partial t} = F(t) - g_L(v - v_L) - M_\infty(v - v_{Ca}) - g_K w(v - v_K) + \left(\frac{L_D}{L_0}\right)^2 \frac{\partial^2 v}{\partial x^2} \tag{24}$$

$$\frac{\partial w}{\partial t} = \frac{(W_\infty - w)}{\tau} \tag{25}$$

$$M_\infty = \frac{1}{2}\left(1 + \tanh\left(\frac{v - v_1}{v_2}\right)\right) \tag{26}$$

$$W_\infty = \frac{1}{2}\left(1 + \tanh\left(\frac{v - v_3}{v_4}\right)\right) \tag{27}$$

$$\tau = \frac{1}{\phi}\operatorname{sech}\left(\frac{v - v_3}{2v_4}\right) \tag{28}$$

Variables v and w represent the transmembrane voltage and gating variable which corresponds to the inhibitory response of the potassium channels. Parameters v_L, v_{Ca}, and v_K are equilibrium potentials for leakage, calcium, and potassium currents, respectively. Factors M_∞ and W_∞ are dimensionless constants which are determined by regulating voltages v_1, v_2, v_3, and v_4. Parameter τ is characteristic time of activation (39). Parameters g_L and g_K are the leakage and potassium conductance scaled relative to the characteristic value of calcium conductance of 20mS (35). With this value of conductance and a typical value of cellular membrane capacitance of 10μF, each unit of dimensionless time in the system of Eqs. (24)-(28) is equivalent to 0.5ms. The value of L_0 in the Eq. (24) is generally ten times greater than the diffusion length $L_D = (D/g_{Ca})^{1/2}$ which is typically equal to 100μm when the diffusion coefficient D is set to a characteristic value of 1μS•cm^2. Thus, the value of parameter $(L_D/L_0)^2$ in the Eq. (24) is equal to 0.01.

The dimensionless length of the BM, L_{BM}, is comprised of the sum of equal lengths of input and output neurons. These lengths are set to 1, except for the Output 2 neuron, which is set to longer 5/3 and shorter 3/2 values for BMA and BMB, respectively (Fig. 18A,B). The lengths of the interneuron are set in the opposite way, to shorter value of 1/2 for BMA (Fig. 28A) and longer value of 2/3 for BMB (Fig. 28B). Synaptic junctions are located at 1/3, 1/2, and 1 to optimize both

distance between synapses and length of the interneuron, allowing excitation waves to fully develop/decay along all segments of the BM.

Figure 18. The Length Scales for the BMA and BMB

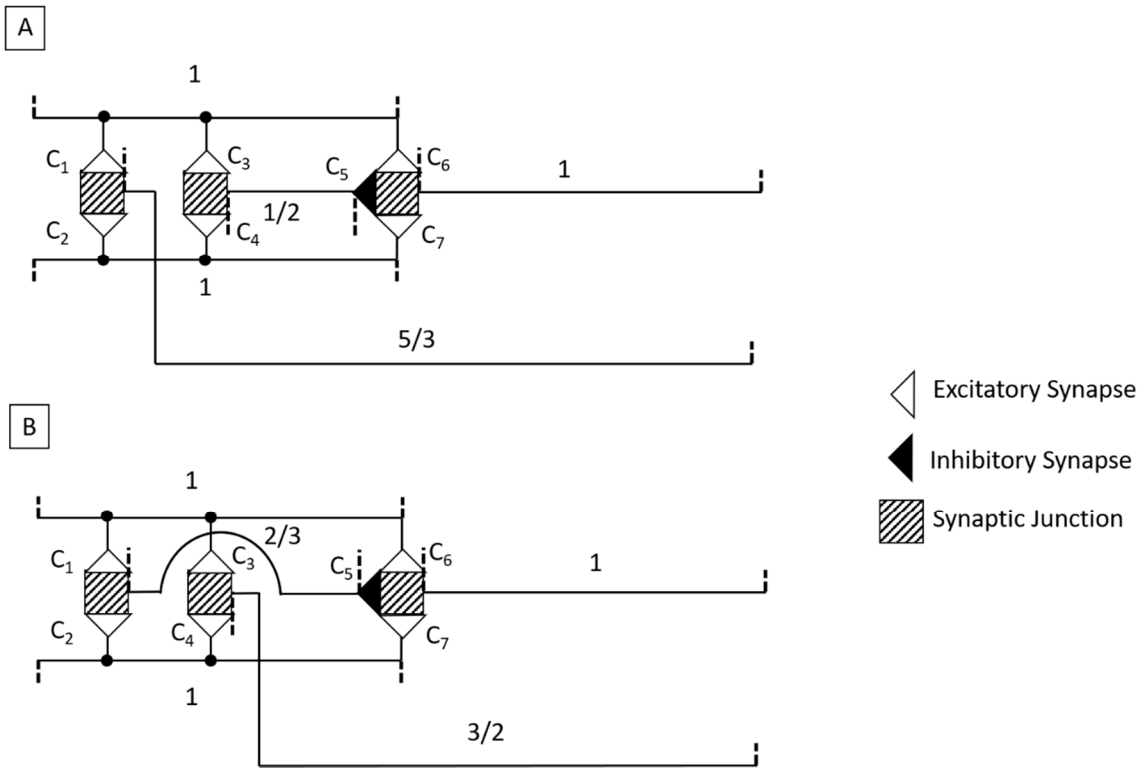

Note Excluding overlapping sections of neurons, the total length of the BM (L_{BM}) is 2. The BMA circuit has a reduced interneuron length of 1/2 and increased Output 2 neuron length of 5/3. The BMB circuit has an increased interneuron length of 2/3 and decreased Output 2 neuron length of 3/2. Synapses are located at 1/3, 1/2, and 1.

The dimensionless amplitude of the stepwise stimulus *F(t)* in the Eq. (24) simulates an activation of the transmembrane potential induced by the external signal incoming from another module or a sensory neuron. The amplitude of *F(t)* and its duration were set to 3 and 2.5, respectively. The stimulus is utilized when the medium is at the equilibrium and is applied between $x = 0$ and $x = 0.15$ in one or both inputs of the BM. Other parameters are set to values given in Table 3.

Table 3. The Parameters of the BM Neuronal Cables Inspired by (39)

ϕ	g_{Ca}	g_K	g_L	v_{Ca}	v_K	v_L	v_1	v_2	v_3	v_4	v_0
0.0167	1	1.8	0.3	1	-0.84	-0.6	-0.012	0.18	0.02	0.30	-0.58

Note The values of parameters remain constant unless stated otherwise.

To complete the system of Eqs. (24)-(28), one needs an additional relationship which would describe the transformation of the excitation wave while it evolves through the synaptic junction. At each of the junctions a Hebbian synaptic equation adjoined with no-flux condition is implemented to ensure that the synapse acts as a unidirectional gate. While the Hebbian synaptic equation is typically nonlinear (36), it can be linearized if sufficient time passes between consecutive input signals to allow the system to return to its resting state. This allows the Hebbian equation to be integrated into existing models more readily.

For neurons with parameters in Table 1 an excitation wave quickly becomes steady state right near the entrance to the BM at a short $x = 0.3$ distance from its input. Indeed, over a period of approximately 60-time units, or 30ms, the transmembrane voltage variable v is nearly 5% away from its equilibrium value (Fig. 19A). As such, within a low range of gamma oscillations in the brain at ~ 30Hz (52), one can treat these waves as a sequence of solitary pulses. Thus, the linear synaptic equation can be utilized, combined with a directional Neumann no-flux condition written as follows

$$v_{post} - v_0 = \sum_{i=1}^{n} C_i\left(v_{i,pre} - v_0\right), \qquad \left.\frac{\partial v}{\partial x}\right|_{x=x_-} = 0 \tag{29}$$

where v_{post} and $v_{i,pre}$ are the post- and pre-synaptic transmembrane potentials, respectively, and x_- is upstream with respect to the direction of the synaptic current. The value of v_0 is the resting transmembrane potential, and C_i is the synaptic strength of the i^{th} synapse in a junction.

Figure 19. The Phase Portrait for the Morris-Lecar Model

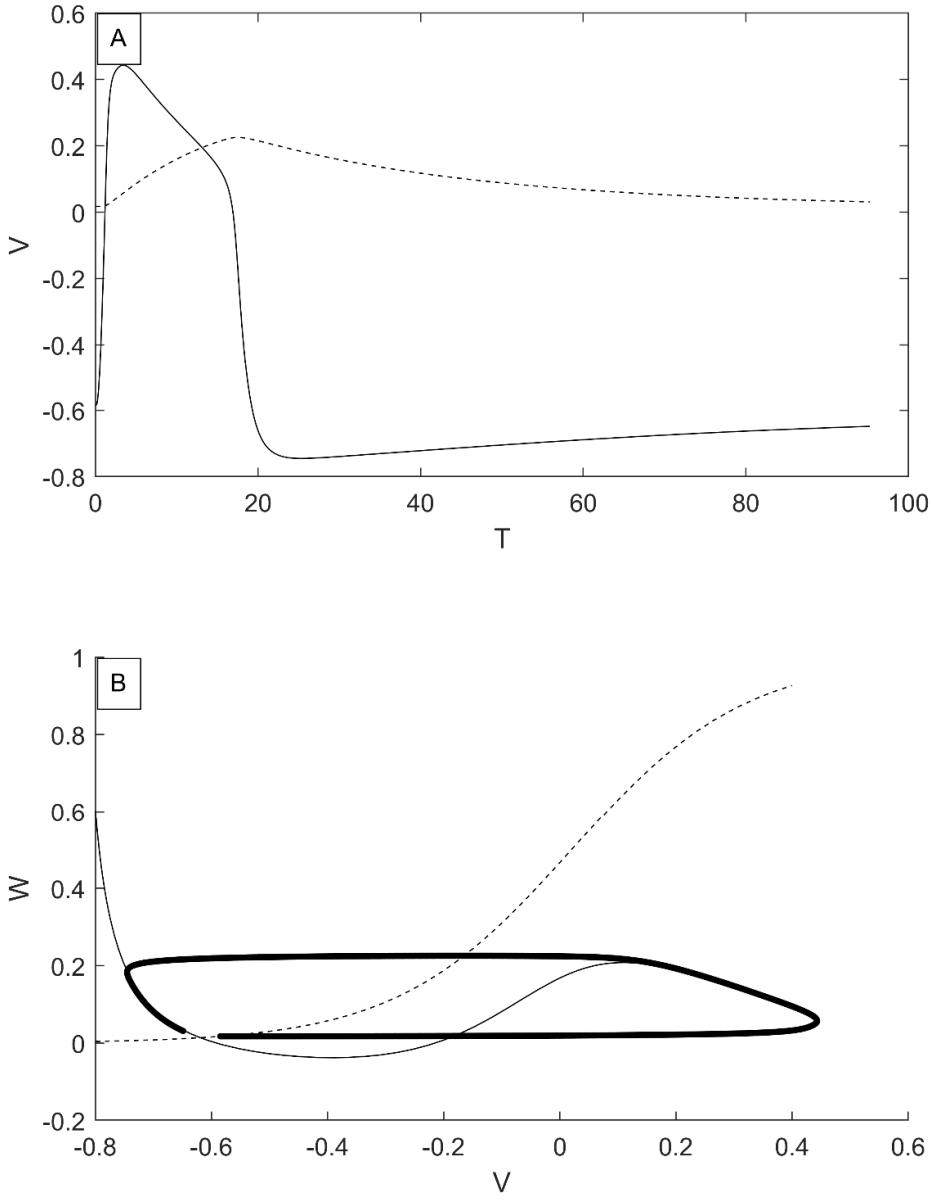

Note A) A fully developed excitation wave in the BM recorded at $x = 0.3$ with parameters $g_k = 2.5$ and $g_L = 0.3$. The solid line represents transmembrane voltage v and the dashed line shows recovery variable w. At the distance $x = 0.3$ away from the BM entrance the wavefront becomes smooth, indicating that the wave is no longer influenced by initial external current $F(t)$. B) Thick

contour depicts a phase trajectory for the steady-state wave propagating in neuronal cables shown in Panel A. Nullclines are indicated as thin and dash contours. The excitation threshold is defined as a difference between the coordinate of intersection of nullclines and the coordinate of intersection of the phase contour with the cubic-like nullcline. This threshold is equal to 0.42.

Equation (29) is applied at all synaptic junctions shown in Fig. 1. At the inputs and outputs of the BM no-flux boundary conditions are implemented, and at four cable intersections marked by dots (Fig. 17) the Eq. (24) like balances with two-dimensional diffusion terms are applied. Since analytical solution of the system of Eqs. (24) - (29) is not possible it is solved numerically using an explicit finite difference method with a first and second order of approximation with respect to time, Δt, and space, Δx, numerical grid intervals. For all numerical experiments the values of these intervals were set to 2.5×10^{-5} and 0.01 for time and space intervals, respectively. Details of discretization of the boundary conditions and numerical solution of the system of Eqs. (24)-(29) have been described in (43).

Numerical solution of Eqs. (24)-(29) can be implemented to study processing of information in the BM. As mentioned above, the focus will be on the assessment of one of the simplest processing sequences such as a single digit addition of two binary input signals and will assume that BMs have equal strengths of excitatory synapses according to Eq. (30)

$$\begin{cases} C_1 = C_2 = C_3 = C_4 \\ C_6 = C_7 \end{cases} \tag{30}$$

Using Eqs. (24)-(30), we will model single digit binary addition using the following essential rules. The first rule is that if any single input stimulus is present, the propagation of the excitation wave in the Output 1 neuron and its absence in the Output 2 neuron determines the binary sum as equal to 1. If no input stimulus is present, then the binary sum is equal to 0. The second rule is that the presence of the excitation wave in the Output 2 neuron and its absence in

the Output 1 neuron implies that two input stimuli are added to each other resulting in the binary sum equal to 0. Concurrently, 1 must be added to the next significant digit in the adjacent BM, if multiple digit addition is considered. These rules can only be upheld in a specific synaptic range.

From the linearity of Eq. (29) and the set of equalities (30), it follows that the first rule is satisfiable if $C_6 = C_7$=1. This condition ensures transmission of a single input stimulus to the Output 1 neuron without changing the steady state character of the propagation of excitation. Likewise, from the linearity of Eq. (29) one can conclude that both rules are satisfiable if $C_1 = C_2 = 0.5$. This restriction ensures either the absence or presence of propagation of a steady state excitation wave in the Output 2 neuron if just one or both BM input stimuli are present, respectively.

Equation (30) entails that the strengths of the other excitatory synapses C_3 and C_4 are also equal to 0.5. So, there is one more steady state excitation wave which is propagating through the inhibitory neuron when both input signals are present. If so, the second rule implies that $C_5 = -2$ to force complete inhibition of the excitation waves propagating through C_6 and C_7, thus ensuring a binary sum of zero in the Output 1 neuron.

The amount of time it takes for an incoming signal to propagate from the BM input neurons to its output neurons is defined as the computational period (CP). The CP is a very important characteristic which determines the BM signal processing speed and is closely related to its spatial extension and the strength of its synaptic connections. The shorter the CP, the higher the processing speed in the BM. However, at certain values of synaptic strength, the mismatch between the excitation wavelength and the spatial scales of the BM can result in processing errors. Under such conditions the signal does not have enough space to completely decay and is still capable of activating synapses in the output- and inter neurons, thus, breaking the described above rules for

binary addition. Such instances of computational volatilities caused by incorrect signal transmission in short BMs will be considered as computational errors with CP set to zero.

It should be noted that since there are two BM output neurons (Fig. 17), one can determine two values of CP. To minimize the influence of the output boundary conditions both values of CP are measured from the onset of the initial stimuli to the moment they reach the points located at L_D away from the ends of output neurons. The greater value will be signified as the BM's CP.

Results and Discussion

Firstly, the dynamics of reaction-diffusion waves were computed to confirm that their evolution through the synapses C_1-C_7 accurately reflects each of the defined above single digit binary addition rules. Figure 20 elucidates the first addition rule with just a single input stimulus present in the BM. Without restriction of generality the stimulus is applied in the Input 2. Panels A-F show propagation of the resulting reaction-diffusion wave from the beginning of the input ($x = 0$) towards the synapse C_7 ($x = 1$). Down the way when the wavefront passes a synapse C_4 (Fig. 20B,G, $t = 2.5$) it initiates a subthreshold excitation at the beginning of the interneuron which decays around inhibitory synapse C_5 without influencing the excitation in the Output 1 neuron (Fig. 20I). In contrast, the excitation initiated by the wave propagating from the Input 2 neuron has a fully developed excitation plateau (Fig. 20C) which, through the synaptic connection C_7, triggers the wavefront in the Output 1 neuron (Fig. 20J). This wavefront propagates further towards the end of the Output 1 neuron (Fig. 20K-Q) and, therefore, produces binary addition yield equal to 1.

Figure 20. Voltage Over Time for the Third Synaptic Junction with a Single Input Present

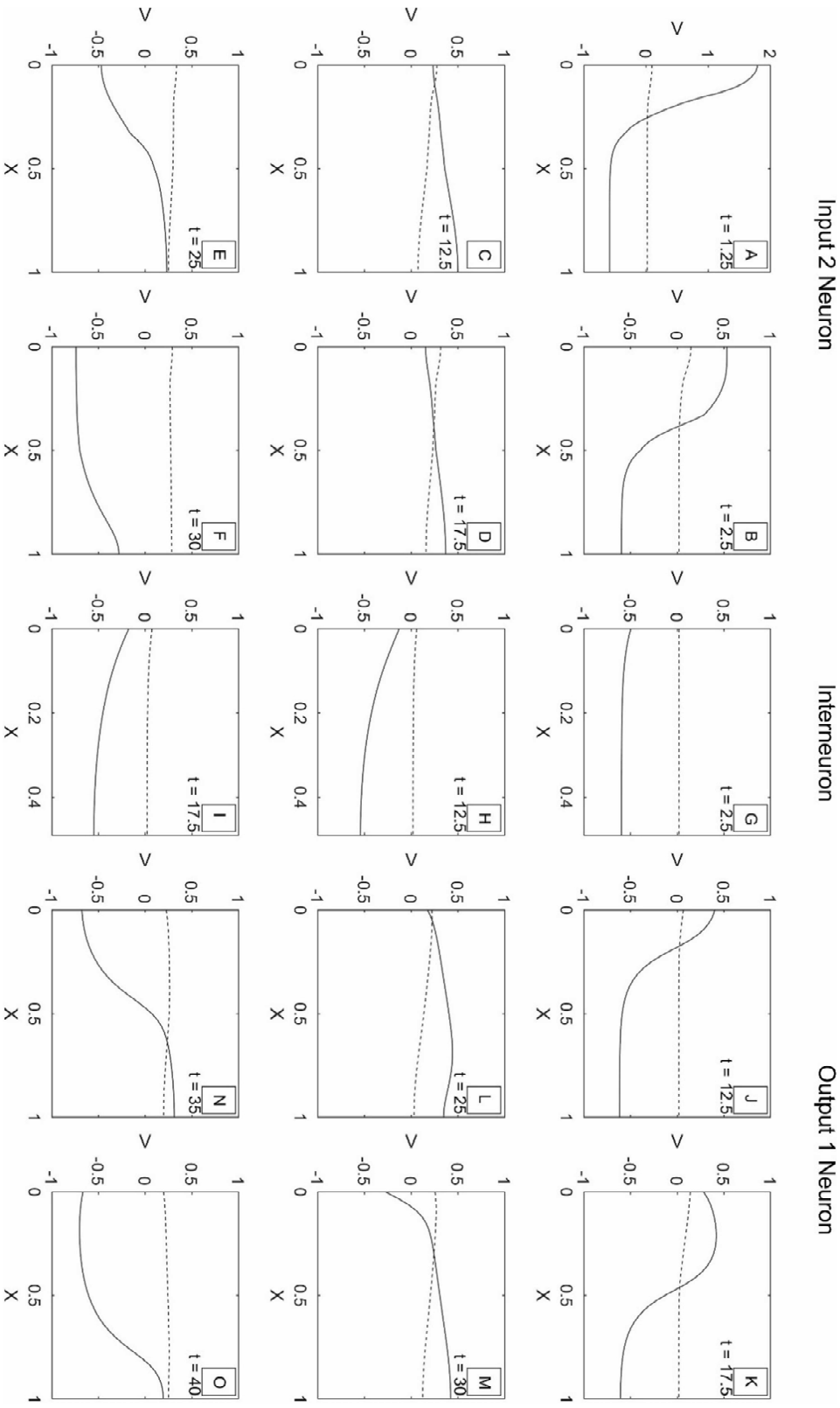

Note A-F correspond to the Input 2 neuron, G-I show the interneuron, and J-O show the Output 1 neuron. Parameters used were $g_K = 1.8$, $g_L = 0.3$, $\phi = 0.0167$.

Figure 21 illuminates the second addition rule when incoming signals are present in both inputs of the BM. Sufficiently fast input reaction-diffusion waves (Fig. 21A) transmit the excitation into the interneuron through the synaptic junction C_3-C_4 (Fig. 21D). Therefore, the resulting reaction-diffusion wave in the interneuron is as developed as both input waves, so all three of them reach synaptic junction C_5-C_7 practically in phase. The balance between inhibitory ($C_5 = -2$) and excitatory ($C_6 = C_7 = 1$) synaptic strengths ensures the absence of excitation in the Output1 neuron, producing binary addition yield equal to 0. In a similar way the transmission of in phase input waves through the synaptic junction ($C_1 = C_2 = 0.5$) results in propagating reaction-diffusion wave in the Output 2 neuron, thus producing a yield equal to 1 which needs to be added to the next significant digit in the adjacent BM unit.

Figure 21. Voltage Over Time for the Third Synaptic Junction when Both Inputs are Present

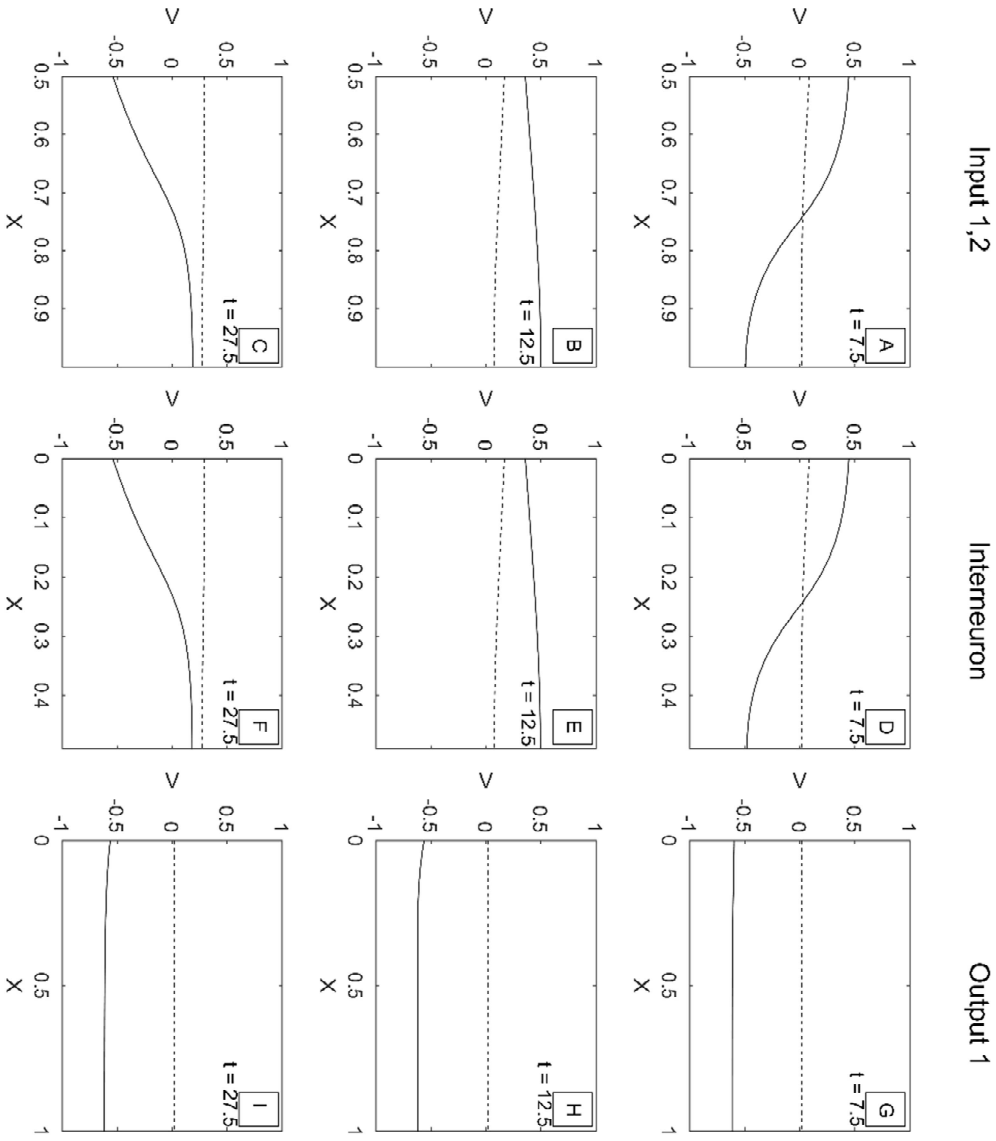

Note A-C corresponds to both Input 1 and 2 neurons, D-F corresponds to the interneuron, and G-I correspond to the Output 1 neuron.

Secondly, to evaluate the speed of binary addition operation described above the values of CP were computed at various BM lengths, different reaction-diffusion parameters, and different synaptic strengths. Unlike previous examples, the strength of excitatory synapses $C_{1\text{-}4}$ in the first two synaptic junctions were varied while other synaptic strengths were still set to constant values $C_5 = -2$, $C_{6\text{-}7} = 1$. The effects of changes of values of parameters on the CP can be seen in Figs. 22-24. As mentioned above, in all these figures zero values of CP correspond to computational errors when under-threshold excitation waves do not properly decay prior to entering the output neurons.

Figure 22. The BMA Computational Periods at Different Reaction-Diffusion Parameters and Different BM Lengths

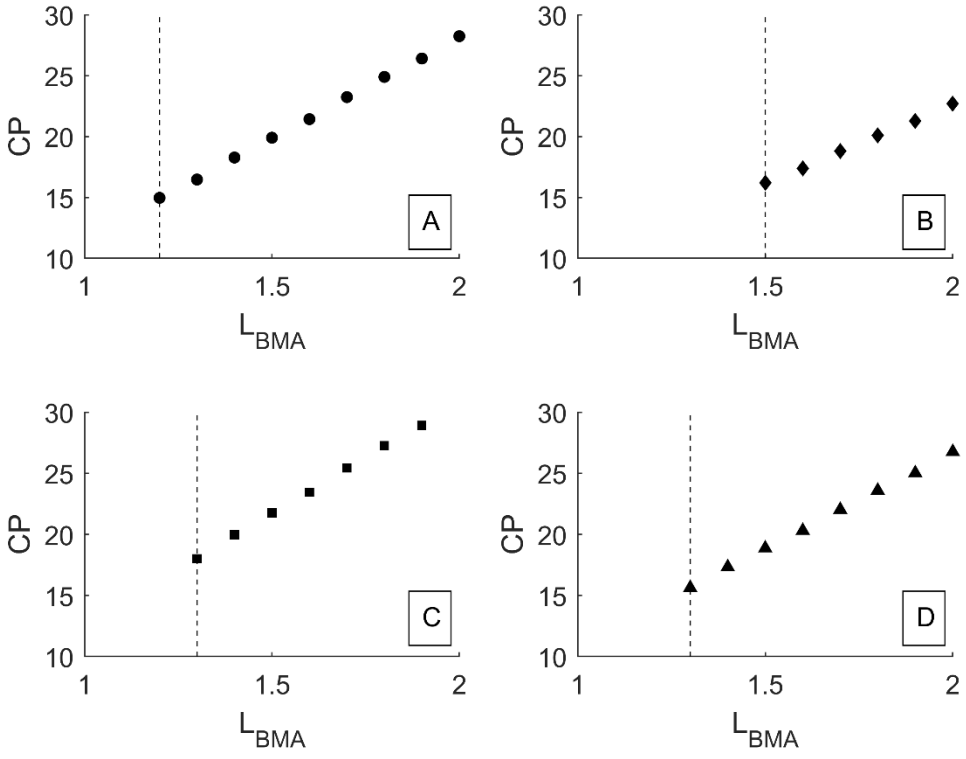

Note Dashed lines represent the lowest length where computational errors still do not occur. Synaptic strengths and set of parameters used are as follows: $C_{1\text{-}4} = 0.5$. A) $g_K = 1.8$, $g_L = 0.3$, $\phi =$

0.0167. B) $g_K = 1.8$, $g_L = 0.2$, $\phi = 0.0167$. C) $g_K = 2.5$, $g_L = 0.3$, $\phi = 0.0167$. D) $g_K = 1.8$, $g_L = 0.3$, $\phi = 0.00167$.

Figure 23. The BMA Computational Periods at Different Parameters $C_{1\text{-}4}$ and Different BM Lengths

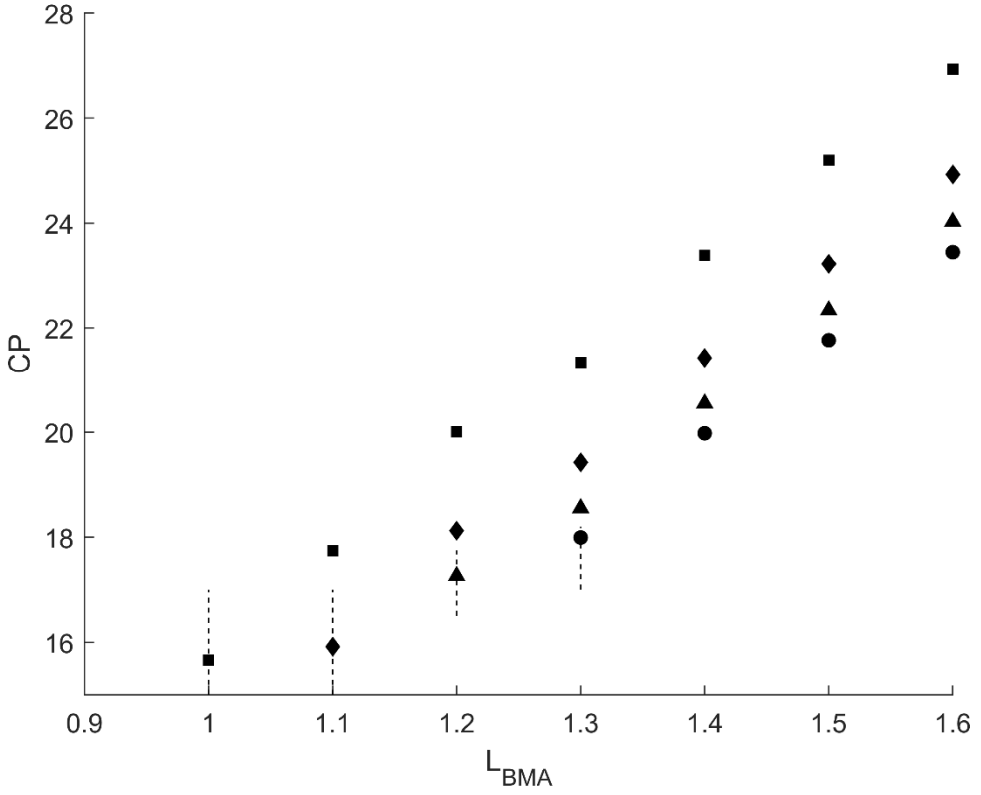

Note Squares, diamonds, triangles, and circles represent $C_{1\text{-}4} = 0.35$, $C_{1\text{-}4} = 0.4$, $C_{1\text{-}4} = 0.45$ and $C_{1\text{-}4} = 0.5$, respectively. Parameters used were $g_K = 2.5$, $g_L = 0.3$, $\phi = 0.0167$.

Figure 24. Dependencies of Computational Periods for the BMA (Dark Gray) and BMB (Light Gray) on Various Values of BMA/BMB Lengths L_{BM} and Synaptic Strengths C_i (i = 1,…,4)

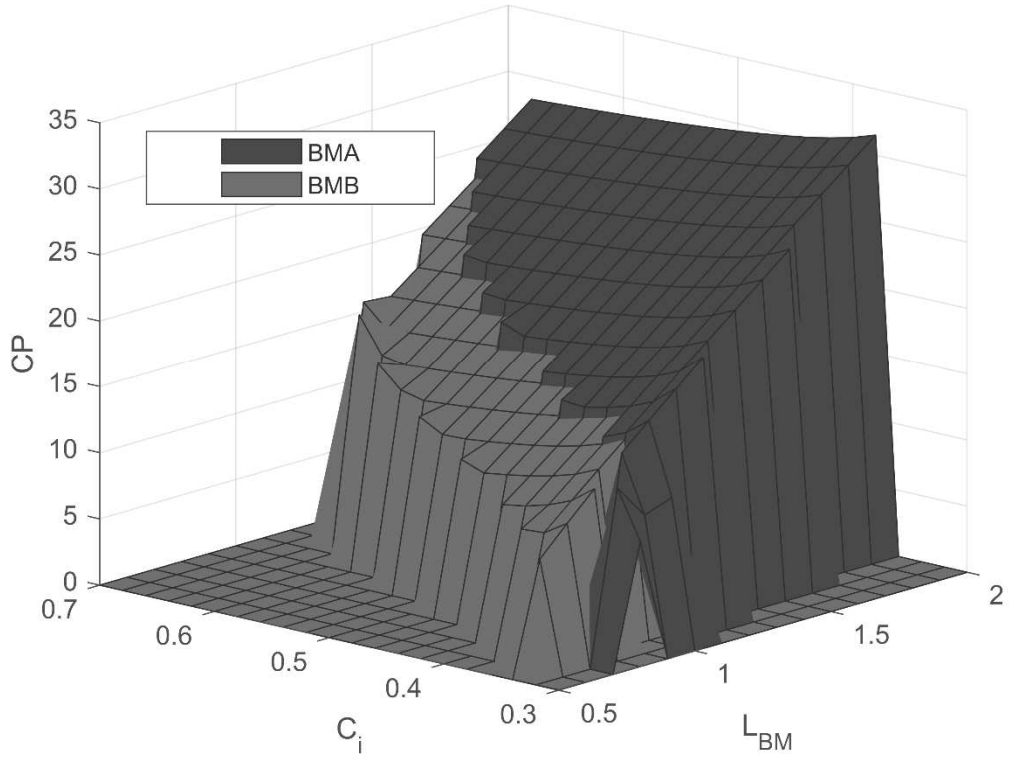

Note Parameters used were $g_K = 2.5$, $g_L = 0.3$, $\phi = 0.0167$.

Figure 22 demonstrates that regardless of a parameter's values the dependences of CP on the length of the BMA are virtually linear. The average slope of these dependences amounts to 15.9 with deviations from the average less than 20%. Although variations in parameter's values did not alter the linear nature of dependences of CP on L_{BMA}, they significantly affected the minimal length of the BMA below which it could not function due to computational errors. For instance, the increase of leakage conductance from 0.2 to 0.3 at constant ϕ and g_K (Fig. 22A,B) resulted in almost a 20% decrease in minimal length allowing the BMA to function at smaller sizes without computational errors. Concurrently, a decrease in potassium conductance and increase in ϕ

decreased the minimal length too, although it did this to lesser extent compared to variations in leakage current (Fig. 22A,C,D). It is important to note that while the minimal value of L_{BMA} noticeably changes in response to variations of BMA parameters, the values of CP do not alter much and fluctuate around 15. Also, at fixed L_{BMA} the greater values of synaptic strengths reduce the CP by the amounts that get gradually saturate at around $C_{1\text{-}4} = 0.5$ (Fig. 23).

Figure 23 shows dependencies of CP on BMA/BMB lengths and parameters $C_{1\text{-}4}$. The range of synaptic strengths at which both types of BM can correctly perform binary calculations significantly decreases for shorter BMs. Higher synaptic strengths generate computational errors at greater BM lengths since the length of the interneuron becomes insufficient to allow appropriate decay of propagating excitation waves. It is worth noticing that CPs tend to increase very abruptly near the boundaries of regions of computational errors, which might explain some computational volatilities associated with severe changes in synaptic strengths due to certain external stressors (53).

As shown in Fig. 24 variations in CP for different synaptic strengths and L_{BM} are quite substantial for both types of BMs. Nonetheless, the BMB's CPs extend to visibly lower values due to greater length of the interneuron. Unlike the strong influence of L_{BM}, the alterations of CP in response to different values of reaction-diffusion parameters are not significant as decreasing ϕ by an order of magnitude and increasing the value of g_K by 40% result only in six and nine percent change in CP, respectively (Fig. 22,23). In general, one could expect greater differences in CP due to changes in reaction diffusion parameters since excitation waves with greater wavelengths typically travel faster. However, in these simulations the BM length as in (43) is significantly shorter than the length of the excitation waves, causing only a segment of the wave being present

in the BM neurons. This in turn results in a more uniform distribution of CP over the range of reaction-diffusion parameters.

Finally, these simulations demonstrate that both types of BMs can perform reliable and quite fast single digit binary operations with CPs ranging between approximately 2 and 25 milliseconds (Fig. 22-24). Concurrently, it is shown that BM lengths vary within nearly three- and eight-millimeters range, so longer BMs correspond to longer calculation periods. The range fits well within the distribution of BM connection lengths in cortical networks of some primates (19) and within determined range of CPs allows to perform binary operations with frequencies in a low range of gamma oscillations in the brain.

To verify the accuracy of results of the computational modeling, excitation waves evolved in response to a single stimulus applied at the beginning of the BMA's Input 2 neuron were used. A comparison was made using different steady-state (t = 2.5 Fig. 20B) grid solutions computed in the Input 2 neuron for a set of Δx varying as 0.02, 0.01, 0.005, 0.0025, and 0.00125. At t = 2.5 the Output 1 neuron was still quiescent, so the difference between solutions was evaluated based on grid values of transmembrane voltage computed only in the Input 2 neuron. The difference between two grid solutions determined at Δx_1 and Δx_2 was calculated as a norm in the space of continuous functions

$$y = \|v\|_c = max_{i=1,\dots,h}\left|v_i^{(1)} - v_i^{(2)}\right| \tag{31}$$

where h is the number of overlapping points between grid solutions v_i computed at Δx_1 and Δx_2. Table 4 shows that the norm y decreases as the difference between spatial scales $x = \Delta x_1 - \Delta x_2$ decreases.

Table 4. Dependence of the Norm y on $x = \Delta x_1 - \Delta x_2$

Spatial scales	$\Delta x_1 = 0.02$ $\Delta x_2 = 0.01$	$\Delta x_1 = 0.01$ $\Delta x_2 = 0.005$	$\Delta x_1 = 0.005$ $\Delta x_2 = 0.0025$	$\Delta x_1 = 0.0025$ $\Delta x_2 = 0.00125$
y	0.0590	0.0290	0.0167	0.0078

Note The dependence shown in Table 4 can be well approximated by a regression line $y = 5.769x + 0.001$ with a high r^2 value of 0.9833. This, in turn, confirms the accuracy of a grid solution v_i which converges to a solution of the nonlinear system of Eqs. (24)-(29) with a sufficiently good degree of convergence of $o(\Delta x)$.

In summary, it was demonstrated that a minimally structured BM can effectively process binary information which propagates through the module's neurons in the form of reaction-diffusion waves. It was found that such millimeter size module may consist of only a few synaptic junctions and neurons and can operate at frequencies typical of low range of gamma oscillations in the brain. It was also determined that BM's calculation speed strongly depends on synaptic strengths and module's size, and only weakly reacts to the alterations of neuronal reaction-diffusion parameters. This suggests that the adaptation of synaptic strengths, which typically occurs during various cognitive processes, may noticeably enhance the computational power of the brain.

CHAPTER IV: CONCLUSIONS AND FUTURE DIRECTIONS

Conclusions

This work demonstrates that reaction-diffusion systems can be used to model both memory and processing functions that are similar to those found in the human brain. The RDMU demonstrates the three core functions of memory: sensitization, habituation, and dishabituation. The RDMU also showed results notably similar to the definitions of PTSD and dementia. This portion is not in the chapter, as there is not much evidence to suggest the RDMU is capable of modelling either of these diseases, yet the similarity is striking enough to warrant interest. Neurons in patients of PTSD become shorter in specific regions of the brain, and responsiveness to fear is increased while suppression of fear is decreased (10,11). Increasing the length of the interneuron causes dishabituation to be significantly harder to achieve, as seen in Fig. 15. As such, the motor neuron is much more responsive to incoming stimuli. Since length is dimensionless, increasing the length of the interneuron can also be interpreted as decreasing the length of both the sensory and the motor neuron. In this way the reduced length of the RDMU, increased responsiveness to stimuli, and reduced ability to habituate correspond to the effects of PTSD.

The RDMU can similarly demonstrate effects that match the definition of dementia. Referring to (12–14), the effects of dementia include the inability to remember recent events, increased number of excitatory synapses, and slower processing speeds. Looking at Fig. 14, one can see that greater synaptic strengths are needed for sensitization to occur when ϕ is 0.017. The lack of sensitization implies that LTP is not taking place, which in turn suggests that information is not being stored. Referring to Fig. 12 shows that the pulse is much weaker for this parameter range, which translates to a slower moving excitation wave and thus decreased processing speeds. While these similarities are not sufficient to claim that the RDMU can model dementia, it is

intriguing that a system as simple as the RDMU can show these effects at all. With a more complicated model and proper experimentation, it could be shown that reaction-diffusion systems are capable of modelling brain-related diseases.

It was shown that the BM is able to model the specific processing task of single-digit binary addition. It is worth noting that the BM performs addition similarly to how an arithmetic logic unit (ALU) performs addition in a computer. As the BM and ALU perform the same task, one could argue that the BM is more efficient as it uses fewer synapses than the ALU uses components (21). Additionally, since the BM and ALU have the same number of inputs, same number of outputs, and both operate in binary, it could be possible to incorporate the BM into current computing systems with minimal modifications once a physical BM has been created.

Future Directions

At present, the three immediate directions this research can take are as follows: 1) combining multiple RDMUs and BMs to perform more complex tasks; 2) implementing equations to allow synapses to automatically adjust strengths according to inputs or lack thereof; and 3) building physical circuits as proof-of-concept in preparation of more complex reaction-diffusion designs.

Progress has already been made for combining multiple BMs to perform multi-digit binary addition, with an existing design (Fig. 25) and an existing framework for experimentation. By connecting the output 2 neuron from the first BM to the synaptic junctions of the second BM, the first BM can transfer specific information to the second BM. In the case of multi-digit binary addition, this information is akin to carrying the 1 in base-10 addition.

Figure 25. The Design for a Multi-Digit Binary Addition BM

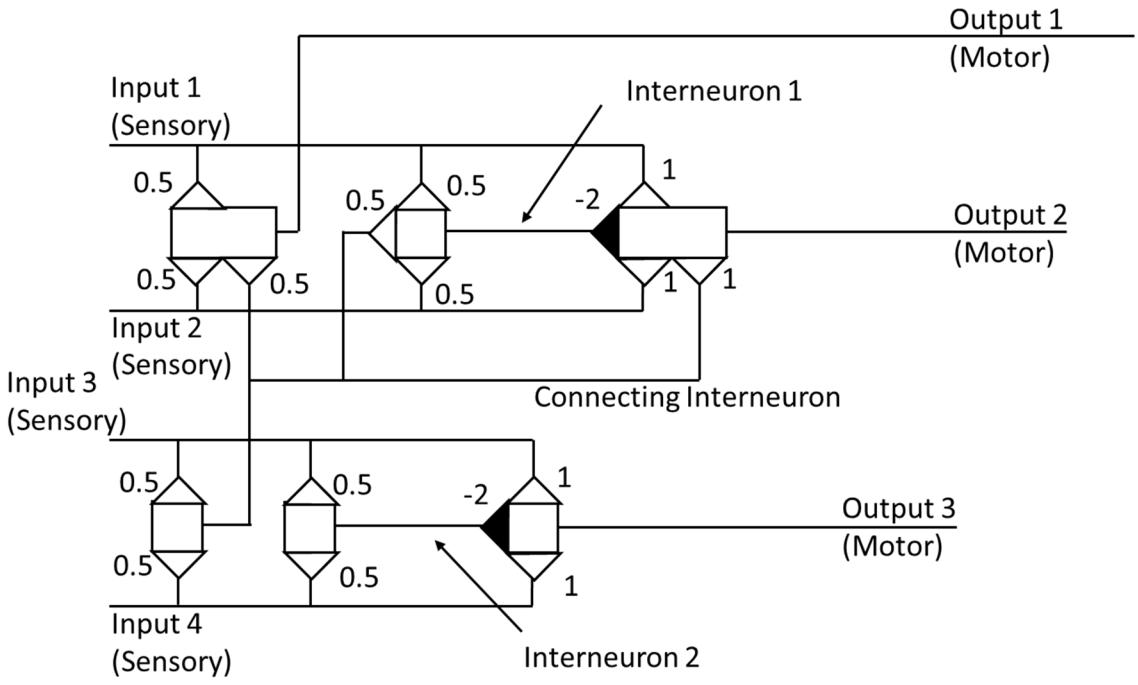

Note The output neuron from one BM becomes an interneuron connecting to all synaptic junctions of the other BM.

Combining modules for more complex tasks may also be used in image processing. While there is currently no intention to pursue reaction-diffusion image processing, as a plethora of better versions are in existence, a theoretical example can still be given (Fig. 26). Using a digital black-and-white image, each pixel in the image can be stored in a RDMU, with a sensitized RDMU representing a black pixel and a habituated RDMU representing a white pixel. The output of the RDMU would connect to one input of a BM, with the other input being the value of the equivalent pixel in the image being compared. If the two pixels are the same, the result of the "addition" is zero, while the result is one if the pixels are different. The output of each BM would connect to a multi-digit addition BM to sum the value of all single-digit BM's, giving a scale of how familiar the comparison image is to the stored image. For example, using 25 pixels for an image, a value

of 0 means the images are identical, while a value of 5 means the images are similar but different. A value of 12 would mean the images are unrelated, and a value of 25 would show that the colors in the images are inverted. This particular setup would take 25 RDMU's and ~30 BM's.

Figure 26. An Example for Reaction-Diffusion Image Processing

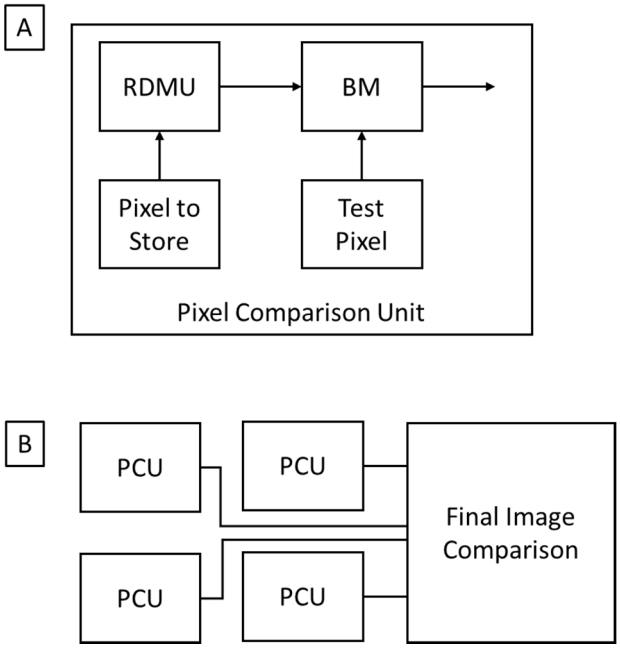

Note A) The pixel to be stored acts as the input for the RDMU, and when a comparison is made the stored pixel and a test pixel become the inputs for the BM. B) The results of the individual comparison are summed, and the result determines how similar the two images are.

The second path this project can take is dynamic synaptic strengths. At present, all synaptic strengths are fixed, and adjustments are made manually. Using naturally adjusting synapses would be useful in modelling memory, as this behavior would more closely mimic the physiological process of memory. The synapses can be made to adjust automatically by introducing a new equation from (36):

$$t_w \frac{dC}{dt} = v_{post} * \left(v_{pre} - v_0\right) \tag{32}$$

where t_w is a time constant for the rate of change of the synaptic strengths, C is the synaptic strength, and v_{post}, v_{pre}, and v_0 are the post-synaptic, pre-synaptic, and resting transmembrane potentials, respectively. This equation was not used in the RDMU because it was not known at the time and was not implemented in the BM because addition required strict, unchanging synaptic strengths. Equation (32) can be easily incorporated into future systems, though experiments will need to be done to optimize the value of t_w.

The third path this project can take is designing a physical circuit. The issue with this path is that with current electronics, information is instantaneously transmitted between components. This precludes propagating waves, and thus feedback and feedforward loops. This problem may be able to be sidestepped with the introduction of a circuit component that requires time for an activity to occur. Once all three paths are followed, this research may hopefully become the base for a new type of artificial intelligence.

REFERENCES

1. Takeuchi T, Duszkiewicz AJ, Morris RGM. The synaptic plasticity and memory hypothesis: Encoding, storage and persistence. Philosophical Transactions of the Royal Society B: Biological Sciences. 2014.

2. Kandel ER, Dudai Y, Mayford MR. The molecular and systems biology of memory. Cell [Internet]. 2014;157(1):163–86. Available from: http://dx.doi.org/10.1016/j.cell.2014.03.001

3. Kandel ER. Dialogue Between Genes and Synapses A Dialogue Between Genes and Synapses. Science (80-). 2007;1030(2001).

4. Halberstadt AL, Geyer MA. Habituation and sensitization of acoustic startle: Opposite influences of dopamine D1 and D2-family receptors. Neurobiol Learn Mem [Internet]. 2009;92(2):243–8. Available from: http://dx.doi.org/10.1016/j.nlm.2008.05.015

5. Rankin CH, Abrams T, Barry RJ, Bhatnagar S, Clayton DF, Colombo J, et al. Habituation revisited: An updated and revised description of the behavioral characteristics of habituation. Neurobiol Learn Mem. 2009;92(2):135–8.

6. Sokolov E. Neuronal models and the orienting influence. 1960;

7. Ramaswami M. Network plasticity in adaptive filtering and behavioral habituation. Neuron. 2014.

8. Marsden KC, Granato M. In Vivo Ca 2+ Imaging Reveals that Decreased Dendritic Excitability Drives Startle Habituation. Cell Rep [Internet]. 2015;13(9):1733–40. Available from: http://dx.doi.org/10.1016/j.celrep.2015.10.060

9. Korn H, Faber DS. The Mauthner cell half a century later: A neurobiological model for decision-making? Neuron. 2005;47(1):13–28.

10. Rubin DC, Berntsen D, Bohni MK. A Memory-Based Model of Posttraumatic Stress Disorder: Evaluating Basic Assumptions Underlying the PTSD Diagnosis. Psychol Rev. 2008;115(4):985–1011.

11. Shiromani PJ, Keane TM, Ledoux J. Post-traumatic stress disorder: Basic science and clinical practice. Post-Traumatic Stress Disorder: Basic Science and Clinical Practice. 2009.

12. Burkart M, Heun R, Benkert O. Serial Position Effects in Dementia. Dement Geriatr Cogn Disord. 1998;9:130–6.

13. Miller SL, Celone K, DePeau K, Diamond E, Dickerson BC, Rentz D, et al. Age-related memory impairment associated with loss of parietal deactivation but preserved hippocampal activation. Proc Natl Acad Sci U S A. 2008;105(6):2181–6.

14. Luszcz MA, Bryana J. Toward understanding age-related memory loss in late adulthood. Gerontology. 1999;45(1):2–9.

15. Bullmore E, Sporns O. The economy of brain network organization. Nat Rev Neurosci. 2012;13(5):336–49.

16. van den Heuvel MP, Sporns O. Network hubs in the human brain. Trends Cogn Sci [Internet]. 2013;17(12):683–96. Available from: http://dx.doi.org/10.1016/j.tics.2013.09.012

17. Pellerin L, Magistretti PJ. How to balance the brain energy budget while spending glucose differently. J Physiol. 2003;546(2):325.

18. Yao Z, Zhang Y, Lin L, Zhou Y, Xu C, Jiang T. Abnormal cortical networks in mild cognitive impairment and alzheimer's disease. PLoS Comput Biol. 2010;6(11).

19. Kaiser M, Hilgetag CC, Van Ooyen A. A simple rule for axon outgrowth and synaptic competition generates realistic connection lengths and filling fractions. Cereb Cortex. 2009;19(12):3001–10.

20. Hagmann P, Cammoun L, Gigandet X, Meuli R, Honey CJ, Van Wedeen J, et al. Mapping the structural core of human cerebral cortex. PLoS Biol. 2008;6(7):1479–93.

21. Plantz RG. Introduction to Computer Organization. 2008. 538 p.

22. Furber S. Large-scale neuromorphic computing systems. J Neural Eng. 2016;13(5).

23. Izhikevich EM. Which model to use for cortical spiking neurons? IEEE Trans Neural Networks. 2004;15(5):1063–70.

24. Borghetti J, Li Z, Straznicky J, Li X, Ohlberg DAA, Wu W, et al. A hybrid nanomemristor/transistor logic circuit capable of self-programming. Proc Natl Acad Sci U S A. 2009;106(6):1699–703.

25. Izhikevich EM. Dynamical Systems in Neuroscience [Internet]. Vol. 25, Dynamical Systems. 2007. 227–256 p. Available from: http://books.google.com/books?hl=en&lr=&id=kVjM6DFk-twC&oi=fnd&pg=PR15&dq=Dynamical+Systems+in+Neuroscience&ots=KRExnXb9si&sig=eN72JzIWk6-LfvNDSFETcxn0vyo

26. Groves PM, Thompson RF. Habituation: A dual-process theory. Psychol Rev. 1970;77(5):419–50.

27. Kandel ER. The Molecular Biology of Memory Storage: A Dialogue Between Genes and Synapses. Science (80-). 2001;294(5544):1030–8.

28. Kandel ER, Tauc L. Mechanism of Heterosynaptic Facilitation in the Giant Cell of the Abdominal Ganglion of Aplysia Depilans. J Physiol. 1965;181:28–47.

29. Malenka RC, Bear MF. LTP and LTD: An embarrassment of riches. Neuron. 2004;44(1):5–21.

30. Gerstner W, Naud R. How Good Are Neuron Models? Science (80-). 2009;326(5951):379–80.

31. Golomb D, Ermentrout GB. Bistability in pulse propagation in networks of excitatory and inhibitory populations. Phys Rev Lett. 2001;86(18):4179–82.

32. Haselwandter CA, Kardar M, Triller A, Da Silveira RA. Self-assembly and plasticity of synaptic domains through a reaction-diffusion mechanism. Phys Rev E - Stat Nonlinear, Soft Matter Phys. 2015;92(3).

33. Adamatzky A, Chua L. Memristor Networks. 2014.

34. Carnevale NT, Hines ML. The NEURON Book. 2006.

35. Morris C, Lecar H. Voltage oscillations in the barnacle giant muscle fiber. Biophys J [Internet]. 1981;35(1):193–213. Available from: http://dx.doi.org/10.1016/S0006-3495(81)84782-0

36. Dayan P, Abbott LF. Theoretical Neuroscience: Computational and Mathematical Modeling of Neural Systems. Computational and Mathematical Modeling of Neural …. 2001.

37. Anokhin K V, Burtsev MS, Ilyin VA, Kiselev II, Kukin KA, Lakhman K V, et al. A review of computational models of neuronal cultures in vitro. Mat Biol Bioinform. 2012;7(2):372–97.

38. Li R, Cao J. Stability analysis of reaction-diffusion uncertain memristive neural networks with time-varying delays and leakage term. Appl Math Comput. 2016;278:54–69.

39. Meier SR, Lancaster JL, Starobin JM. Bursting regimes in a reaction-diffusion system with action potential-dependent equilibrium. PLoS One [Internet]. 2015;10(3):1–25. Available from: http://dx.doi.org/10.1371/journal.pone.0122401

40. Shuman T, Amendolara B, Golshani P. Theta Rhythmopathy as a Cause of Cognitive Disability in TLE. Epilepsy Curr. 2017;17(2):107–11.

41. Buzsaki G. Theta Oscillations in the Hippocampus. Neuron. 2002;33:325–40.

42. Bean BP. The action potential in mammalian central neurons. Nat Rev Neurosci. 2007;8(6):451–65.

43. Carnaghi MM, Starobin JM. Reaction-diffusion memory unit: Modeling of sensitization, habituation and dishabituation in the brain. PLoS One [Internet]. 2019;14(12):1–16. Available from: http://dx.doi.org/10.1371/journal.pone.0225169

44. Firmin L, Field P, Maier MA, Kraskov A, Kirkwood PA, Nakajima K, et al. Axon diameters and conduction velocities in the macaque pyramidal tract. J Neurophysiol. 2014;112(6):1229–40.

45. Neuhuber B, Timothy Himes B, Shumsky JS, Gallo G, Fischer I. Axon growth and recovery of function supported by human bone marrow stromal cells in the injured spinal cord exhibit donor variations. Brain Res. 2005;1035(1):73–85.

46. Hawkins RD, Cohen TE, Kandel ER. Dishabituation in Aplysia can involve either reversal of habituation or superimposed sensitization. Learn Mem. 2006;13(3):397–403.

47. Antonov I, Kandel ER, Hawkins RD. The contribution of facilitation of monosynaptic PSPs to dishabituation and sensitization of the Aplysia siphon withdrawal reflex. J Neurosci. 1999;19(23):10438–50.

48. Castellucci V, Pinsker H, Kupfermann I, Kandel ER. Neuronal Mechanisms of Habituation and Dishabituation of the Gill-Withdrawal Reflex in Aplysia. Science (80-). 1970;167(3926):1745–8.

49. Marcus EA, Nolen TG, Rankin CH, Carew TJ. Behavioral Dissociation of Dishabituation, Sensitization, and Inhibition in Aplysia Published by : American Association for the Advancement of Science Stable URL : https://www.jstor.org/stable/1701145 REFERENCES Linked references are available on JSTOR. 1988;241(4862):210–3.

50. Cohen TE, Kaplan SW, Kandel ER, Hawkins RD. A simplified preparation for relating cellular events to behavior: Mechanisms contributing to habituation, dishabituation, and sensitization of the Aplysia gill-withdrawal reflex. J Neurosci. 1997;17(8):2886–99.

51. Adamatzky A, Costello BDL, Asai T. Reaction-Diffusion Computers. Reaction-Diffusion Computers. 2005.

52. Axmacher N, Mormann F, Fernández G, Elger CE, Fell J. Memory formation by neuronal synchronization. Brain Research Reviews. 2006.

53. Kasanetz F, Deroche-Gamonet V, Berson N, Balado E, Lafourcade M, Manzoni O, et al. Transition to addiction is associated with a persistent impairment in synaptic plasticity. Science (80-). 2010;